

Self-Training Guided Disentangled Adaptation for Cross-Domain Remote Sensing Image Semantic Segmentation

Qi Zhao, *Member, IEEE*, Shuchang Lyu, *Graduate Student Member, IEEE*, Binghao Liu, Lijiang Chen, *Member, IEEE*, Hongbo Zhao, *Senior Member, IEEE*

Abstract—Remote sensing (RS) image semantic segmentation technology has achieved great success used in many real-world applications such as geographic element analysis. With well-trained deep convolutional neural networks (DCNNs), the performance on RS image semantic segmentation task reaches high-level. However, strong dependency on annotated data of specific scene makes it hard for DCNNs to fit different RS scenes. To solve this problem, recent works gradually focus on cross-domain RS image semantic segmentation task. In this task, different ground sampling distance, remote sensing sensor variation and different geographical landscapes are three main factors causing dramatic domain shift between source and target images. To decrease the negative influence of domain shift, we propose a self-training guided disentangled adaptation network (ST-DASegNet). We first propose source student backbone and target student backbone to respectively extract the source-style and target-style feature for both source and target images. Towards the intermediate output feature maps of each backbone, we adopt adversarial learning for alignment. Then, we propose a domain disentangled module to extract the universal feature and purify the distinct feature of source-style and target-style features. Finally, these two features are fused and served as input of source student decoder and target student decoder to generate final predictions. Based on our proposed domain disentangled module, we further propose exponential moving average (EMA) based cross-domain separated self-training mechanism to ease the instability and disadvantageous effect during adversarial optimization. Extensive experiments and analysis on benchmark RS datasets (Potsdam, Vaihingen and LoveDA) show that ST-DASegNet outperforms previous methods on cross-domain RS image semantic segmentation task and achieves state-of-the-art (SOTA) results. Our code is available at <https://github.com/cv516Buaa/ST-DASegNet>.

Index Terms—Remote sensing image semantic segmentation, Unsupervised domain adaptation, Self-training, Domain disentangling, Adversarial learning

I. INTRODUCTION

REMOTE sensing (RS) technology has been broadly applied in many real-world vision applications, such as remote sensing scene classification [1]–[5], object detection [6]–[8], semantic segmentation [9]–[11], etc. Among the above applications, remote sensing scene image semantic segmentation is a popular research direction, which aims to

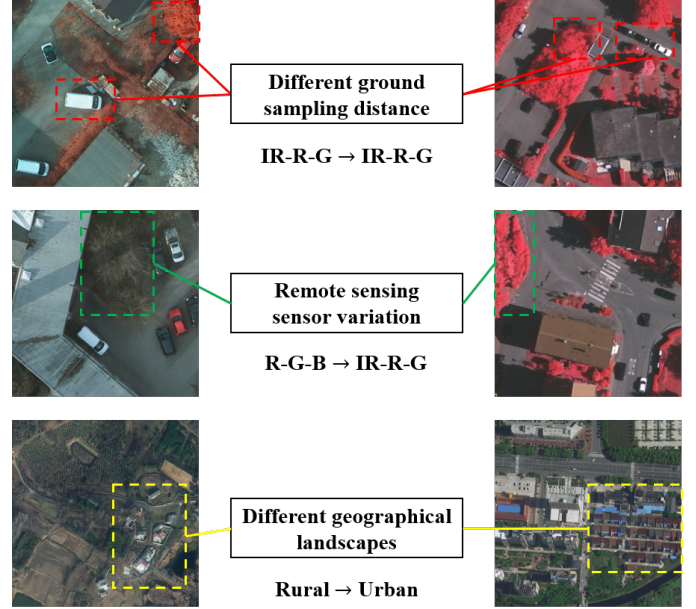


Fig. 1. Intuitive cases to explain the main problems in cross-domain remote sensing image semantic segmentation.

predict an accurate category for each pixel of RS scene images. Recently, the development of DCNNs [12]–[16] boosts the performance of RS image semantic segmentation task. However, the powerful performance heavily relies on the large amount of annotated training samples, which have close data distribution with testing samples. In practical applications, the scene of testing (target) images always has drastic variation with the scene of training (source) images. To decrease the domain shift and bridge the domain gap between source and target images, cross-domain RS image semantic segmentation becomes a hot topic.

Cross-domain semantic segmentation task mainly aims at using a model trained with source images to generate pixel-wise predictions on target images, where source and target images have obvious discrepancy causing heavily domain shift problem. To solve this problem, many notable methods have been proposed on natural scene images [17]–[21]. Different from natural scene images, the domain shift problems of RS images mainly result from different ground sampling distance, remote sensing sensor variation and different geographical landscapes. As shown in Fig.1, different ground sampling

Corresponding Author: Hongbo Zhao

Qi Zhao, Shuchang Lyu, Binghao Liu, Lijiang Chen and Hongbo Zhao are with the Department of Electronics and Information Engineering, Beihang University, Beijing, 100191, China, (e-mail: zhaohq@buaa.edu.cn, lyushuchang@buaa.edu.cn, liubinghao@buaa.edu.cn, chenlijiang@buaa.edu.cn, bhzhb@buaa.edu.cn).

distance brings in severe scale variation. Remote sensing sensor variation directly enlarges the appearance discrepancy on some specific categories between source and target images (E.g., “Tree” on R-G-B and IR-R-G images shows different colors.). Different geographical landscapes make element of same category shows different characteristics (E.g., “rural building” has different patterns with “urban building”).

To decrease the domain shift and improve the representation generalization on cross-domain RS image semantic segmentation task, we propose four principles as theoretical instruction of our method. (1) From the intuitive view of human vision system, RS images from different domains have large visual discrepancy. However, it is not hard for us to distinguish geographical elements. It means that images from different domains contain both unique and invariant (universal) features. (2) RS images always cover large geographical area, so we intuitively infer that image-level alignment using generation techniques (E.g., image translation) may become harder and feature-level alignment may be better. (3) RS images always contain complex geographical information. Therefore, directly applying adversarial learning mechanism may make the training process suffer from instability. (4) Even though adversarial learning can largely fill the domain gap, but lacking target annotations still leads to representation tendency on source images. Based on the above-mentioned principles, we propose a novel Self-Training Guided Disentangled Adaptation Network (ST-DASegNet) to tackle the cross-domain RS image semantic segmentation task.

Following the first two principles, we design a Disentangled Adaptation Network (DASegNet). Specifically, we first design two student backbones to represent source and target images in two-style. Source student backbone is designed to respectively represent source and target image as “source-domain source-style feature” and “target-domain source-style feature”. Target student backbone is designed to respectively represent source and target image as “source-domain target-style feature” and “target-domain target-style feature”. With this design, we expect to obtain a target-sensitive backbone, which is more suitable for target images. Then, towards cross-domain single-style features (source and target output features from same student backbone), we adopt adversarial learning for feature-level alignment. This can explore the potential of student backbones to adapt source annotations to target domain. Next, towards single-domain cross-style features (source or target output features from different student backbones), we propose Domain Disentangled Module (DDM) to extract the universal feature and purify distinct feature by fusion and disentangling operations. Finally, we design source student decoder and target student decoder to respectively map source-style and target-style feature into final predictions. During optimizing with only source labeled samples, target student backbone and decoder tend to be more sensitive to target-style features. It means target student can find the instinct target-style features in both source and target images. Intuitively, target image contains more instinct target-style features than source image, so target student can represent target image better. Similarly, source student is more suitable for source images.

Following the last two principles, we propose an EMA

based cross-domain separated self-training paradigm to further rectify the representation tendency and stabilize optimization. Teacher model of previous self-training paradigm is always an EMA of the student model. In our “decoder-only” paradigm, we only use two teacher decoders (Source teacher decoder and target teacher decoder) instead of whole teacher network. This efficient “decoder-only” paradigm can save a lot of training memory and computation cost because decoder of a segmentation network is always much smaller than backbone. Here, we propose another self-training paradigm, which is “single-target” paradigm. In this paradigm, we apply target teacher backbone and target teacher decoder for pseudo label generation. “Single-target” paradigm provides another perspective on integrating self-training mechanism into DASegNet. EMA based cross-domain separated self-training paradigm can smoothly integrate into DASegNet and form the final ST-DASegNet.

To verify the performance of ST-DASegNet, we conduct extensive experiments on benchmark datasets (Potsdam/Vaihingen [22] and LoveDA [23]). Comparison experiments show that ST-DASegNet outperforms previous methods and achieves SOTA results. Visualization and analysis further show the interpretability of ST-DASegNet.

In summary, the main contributions are listed as follows:

- To solve the domain shift problem on cross-domain RS image semantic segmentation task, we propose a self-training guided disentangled adaptation network (ST-DASegNet) with outstanding representation generalization.
- We propose a domain disentangled module to extract the cross-domain universal feature and purify the single-domain distinct feature, which provides an insight on utilizing feature disentangling to bridge domain gap.
- We propose an efficient EMA based cross-domain separated self-training paradigm and integrate it with adversarial learning. This design can rectify the representation tendency and stabilize optimization.
- Extensive experiments show that our proposed ST-DASegNet achieves SOTA results than previous methods on multiple notable benchmark datasets.

II. RELATED WORK

A. Remote Sensing Image Semantic Segmentation

Semantic segmentation is a classical computer vision task, which plays an important role in many real-world applications. Fully convolutional networks (FCN) [12] first proposes an end-to-end deep learning architecture for semantic segmentation. From then, many notable generalized segmentation networks [13]–[15], [24]–[28] are directly applied and fitted in well on RS images.

With the development of RS technology, remote sensing image semantic segmentation gradually becomes popular research topic. Compared to natural scene images, remote sensing images contain more specific detailed information like element boundary and corner, irregular shape, etc. Moreover, large geographical coverage and confusing geographical elements on RS images causes large intra-class variance and inter-class similarity. On solving these problems, many novel and

strong RS segmentation networks are proposed. Li *et al.* [29] propose a novel adaptive multi-scale deep fusion (AMDF) ResNet to fuse multiple hierarchy features in an adaptive manner. With abundant and discriminative feature extraction, AMDF-ResNet achieves high-level performance. Nogueira *et al.* [30] propose an efficient dilated network, which improves the network by exploring the multi-context features. Besides exploiting the effective information on multiple features, some works focus on integrating attention mechanism into RS segmentation networks. [31]–[33] utilize spatial-wise and channel-wise attention modules, which can overcome confusing recognition by capturing long-range spatial relationships and selecting more important channels. [34]–[37] all pay attention to boundary parsing. These edge-sensitive architectures offer an inspiring perspective on enhancing the understanding of more complex geographical elements in pixel-wise.

B. Unsupervised Domain Adaptation for Cross-domain Semantic Segmentation

With domain shift alleviating mechanism, unsupervised domain adaptation (UDA) techniques can make a source-trained (trained only with source samples) models adapt to target samples. Recently, many remarkable works have made huge progress on applying UDA on cross-domain semantic segmentation task.

Adversarial learning is frequently adopted in many excellent methods. Some methods utilize image generalization techniques like image translation [19], [38] to align image appearance between source and target images. [39]–[43] employ image-level adaption in the first step and then train the segmentation networks with cross-domain synthetic data. Other methods explore the domain-invariant features between source-style and target-style features, which takes advantage of feature-level alignment strategy to solve the domain shift problem. [44]–[47] insert discriminators into networks for consistency alignment on intermediate feature maps or output entropy maps.

As another typical non-adversarial UDA paradigm, self-training has attracted many attentions in cross-domain semantic segmentation task. [20], [21], [48], [49] promote the adaption ability by generating reliable, consistent and class-balanced pseudo labels. Supervised by target pseudo ground-truth, models can quickly adapt to target images in quick and stable manner.

C. Cross-domain Remote Sensing Image Semantic Segmentation

Although cross-domain RS image semantic segmentation task has not been fully studied and the cross-domain adaptive potential has not been fully exploited, there are still many awesome works proposed in recent years. Benjdira *et al.* [50] first addresses domain adaptation issue for RS image semantic segmentation task. They use generative adversarial networks (GANs) based architecture to tackle this task and achieve convincing results. Followed their pioneer work, Li *et al.* [51] introduce DualGAN [52] and demonstrate its strong adaptation ability on RS image semantic segmentation

task. Similarly, [53]–[55] all design GANs-based network and explore the adaptive potential of GANs on cross-domain RS image semantic segmentation task. Bai *et al.* [56] propose a novel network integrating adversarial learning and contrastive learning. Combined with adversarial loss and pixel-wise contrastive loss, the segmentation network can learn rich domain-invariant features. Wu *et al.* [57] also focus on extracting domain-invariant features. Instructed by this principle, they propose a deep covariance alignment (DCA) module, which achieves competitive results on famous benchmark dataset, LoveDA [23]. Li *et al.* [58] propose a step-wise RS segmentation networks with covariate shift alleviation close the gap between source and target domains. Zhang *et al.* [59] propose a curriculum-style local-to-global RS segmentation framework. It designs a two-stage cross-domain adaptation process, which are “source domain to Easy-to-adapt” and “Easy-to-adapt to Hard-to-adapt”. All the above-mentioned brilliant works advance the cross-domain RS image semantic segmentation task.

III. PROPOSED METHOD

To decrease the negative influence of domain shift between source and target RS image, we propose a self-training guided disentangled adaptation network (ST-DASegNet). The overview of ST-DASegNet is shown in Fig.2. In this paper, we follow the unsupervised domain adaptation constraint, which means annotations of source samples are given while no annotation of target samples is available.

A. Source and Target Student Backbones

From our proposed first principle in Sec.I, we believe that unique features lead to large visual discrepancy while invariant features lead to easy identification. Naturally, if the model can precisely extract two-style features from two-domain images, it will benefit to unique and invariant feature representation. Motivated by this reasonable assumption, we design two student backbones rather than common-applied weight-sharing backbone. Here, the source student backbone (B_S) is expected to extract source-style features from two-domain images. Similarly, the target student backbone (B_T) is expected to extract target-style features from two-domain images.

As shown in Fig.2, source and target images (x_s and x_t) will be respectively fed into the source and target student backbones. Eq.1 and Eq.2 show this process.

$$F_{S-s} = B_S(x_s), \quad F_{S-t} = B_S(x_t) \quad (1)$$

$$F_{T-s} = B_T(x_s), \quad F_{T-t} = B_T(x_t) \quad (2)$$

where F_{S-s} and F_{S-t} are two output features from source student backbone, which respectively denote source-domain source-style feature and target-domain source-style feature. F_{T-s} and F_{T-t} are two output features from target student backbone, which respectively denote source-domain target-style feature and target-domain target-style feature.

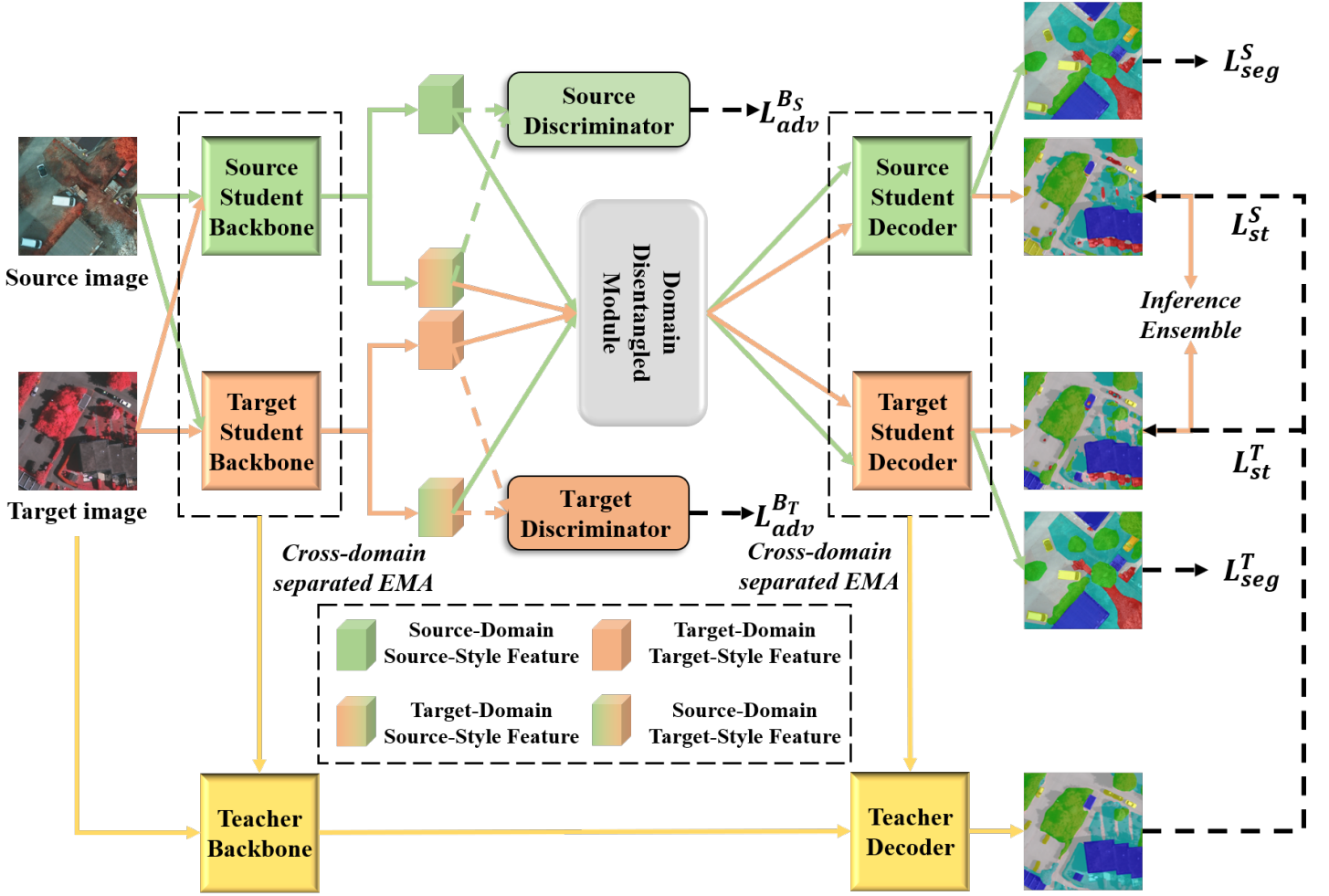


Fig. 2. **The overview of ST-DASegNet.** In this architecture, source and target student backbones are designed for feature extraction on two-style features. Domain disentangled module is designed to extract the cross-domain universal features and single-domain unique features. Source and target student decoders are designed to respectively map source and target features into predictions. Teacher backbone and decoder are respectively updated by student backbones and student decoders with EMA technique. D_{SS} and D_{TS} are two discriminators to align cross-domain same-style features.

B. Adversarial Learning on Cross-Domain Single-Style Features

From our proposed second principle in Sec.I, we believe that feature-level alignment may be more suitable than image-level alignment on cross-domain RS image semantic segmentation task. Feature alignment can guarantee the basic adaptation ability of student backbones and enhance the representation consistency between cross-domain images. In this paper, we design two discriminators to apply adversarial learning on cross-domain single-style features. Specifically, source discriminator (D_S) is proposed to align source-domain source-style feature and target-domain source-style feature. target discriminator (D_T) is proposed to align source-domain target-style feature and target-domain target-style feature. The mathematical operations are shown in Eq.3 and Eq.4.

$$\mathcal{L}_{adv}^{B_S}(B_S, D_S) = \mathbb{E}_{x^s \sim X^s} [\log(D_S(\mathbf{F}_{S-s}))] + \mathbb{E}_{x^t \sim X^t} [\log(1 - D_S(\mathbf{F}_{S-t}))] \quad (3)$$

$$\mathcal{L}_{adv}^{B_T}(B_T, D_T) = \mathbb{E}_{x^t \sim X^t} [\log(D_T(\mathbf{F}_{T-t}))] + \mathbb{E}_{x^s \sim X^s} [\log(1 - D_T(\mathbf{F}_{T-s}))] \quad (4)$$

where $\mathcal{L}_{adv}^{B_S}(B_S, D_S)$ and $\mathcal{L}_{adv}^{B_T}(B_T, D_T)$ are adversarial losses. To optimize B_S and B_T . We adopt “min-max” criterion, which can be expressed in Eq.5.

$$\begin{cases} \min_{B_S} \max_{D_S} \mathcal{L}_{adv}^{B_S}(B_S, D_S) \\ \min_{B_T} \max_{D_T} \mathcal{L}_{adv}^{B_T}(B_T, D_T) \end{cases} \quad (5)$$

C. Domain Disentangled Module on Single-Domain Cross-Style Features

From source and target student backbones, we can obtain two-style features for source and target images. With feature-level adversarial learning on these features, domain shift problem is alleviated. Naturally, we prepare to extract universal and unique features from single-domain cross-style features. In this paper, we propose a domain disentangled module (DDM). The module structure is shown in Fig.3.

In DDM, two input features are extracted by two student backbones from single domain image, so two features have different styles. Here, we first propose a common fusion block

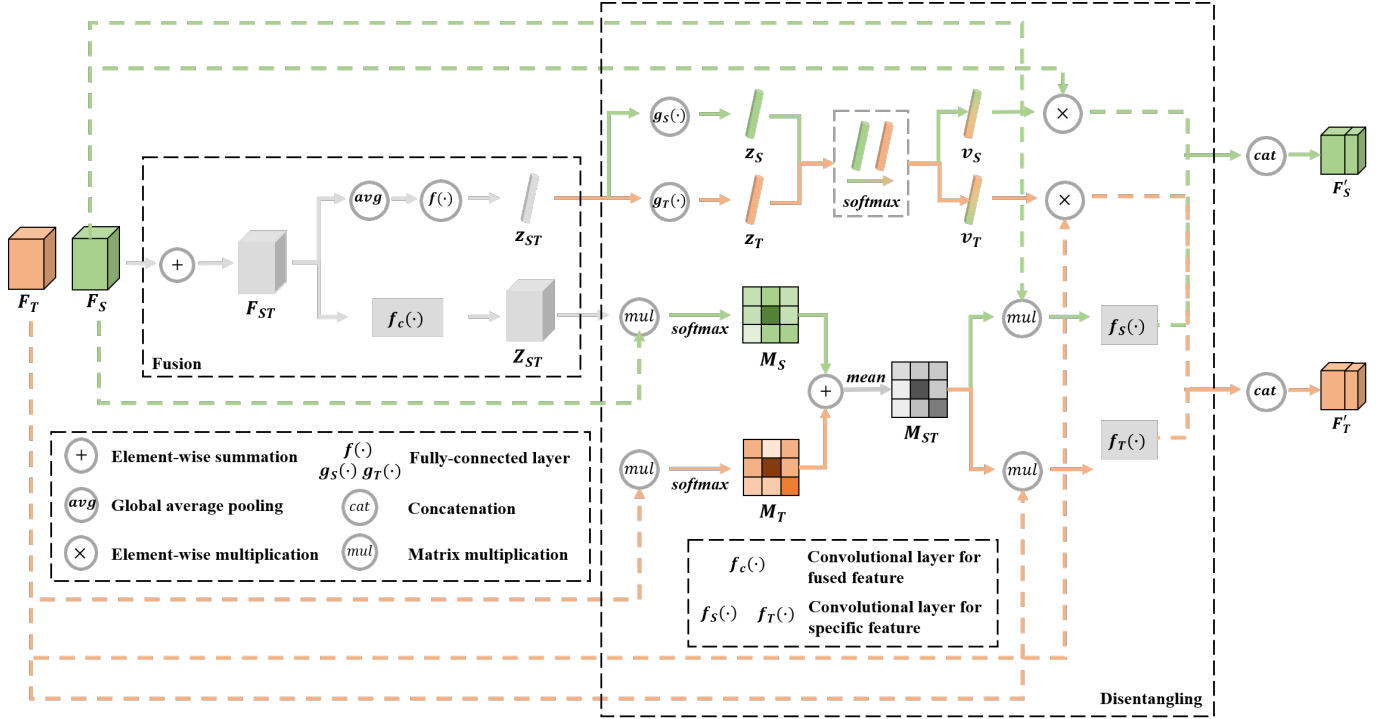


Fig. 3. **The module structure of domain disentangled module.** In this module, F_S and F_T respectively denote source-style and target-style features. Particularly, two features are extracted from single-domain image (E.g., F_{S-s} and F_{T-s}). This module consists of fusion and disentangling blocks. Fusion block is used to generate a fused prototype and feature map. In disentangling block, fused prototype is used to generate unique feature while fused feature map is used to generate invariant feature. Finally, there two features are concatenated together.

to generate fused prototype (z_{ST}) and fused feature map (Z_{ST}). The detailed process of fusion block is shown in Eq.6.

$$z_{ST} = f(\text{avg}(F_{ST})), \quad Z_{ST} = f_c(F_{ST}) \quad (6)$$

As shown in Fig.3, $f(\cdot)$ denotes a fully-connected layer (dimensionality-reduction). $f_c(\cdot)$ denotes a convolutional layer. $\text{avg}(\cdot)$ denotes channel-wise global average pooling operation. $F_{ST} = F_S + F_T$.

We then propose a disentangling block to decouple unique and invariant features. This block can be separated into two parts. The first part is designed to extract unique feature. Even if source student and target student backbone can represent single-domain image as source and target styles, the output features are still mixtures partially containing other style feature (E.g., source-domain source-style feature contains some target-style information). Therefore, unique feature extraction can be regarded as purifying the style-specific feature from fused feature. As shown in Fig.3, z_{ST} is served as a guided prototype to generate two complementary vectors (v_S and v_T). The generation process is shown in Eq.7 and Eq.8.

$$v_S = \frac{\exp(z_S)}{\exp(z_S) + \exp(z_T)}, \quad v_T = \frac{\exp(z_T)}{\exp(z_S) + \exp(z_T)} \quad (7)$$

$$z_S = g_S(z_{ST}), \quad z_T = g_T(z_{ST}) \quad (8)$$

where $g_S(\cdot)$ and $g_T(\cdot)$ are two style-specific fully-connected layers (dimensionality-increase). $v_S + v_T = 1$. Eq.7 shows softmax operation.

With v_S and v_T , we conduct channel-wise multiplication on input features (F_S and F_T). Here, $v_S = [v_S^1, v_S^2, \dots, v_S^C]$.

$v_T = [v_T^1, v_T^2, \dots, v_T^C]$. $F_S = [F_S^1, F_S^2, \dots, F_S^C]$. $F_T = [F_T^1, F_T^2, \dots, F_T^C]$. Eq.9 shows the channel-wise multiplication operation.

$$F_{U-S}^i = F_S^i \times v_S^i, \quad F_{U-T}^i = F_T^i \times v_T^i \quad (9)$$

where v_S^i and v_T^i are scalars of v_S and v_T (\mathbb{R}^C). F_S^i and F_T^i ($\mathbb{R}^{H \times W}$) are channels of F_S and F_T ($\mathbb{R}^{C \times H \times W}$). F_{U-S} and F_{U-T} are respectively source-style and target-style unique features.

The second part of DDM is designed to extract invariant features. The key idea of this part is to find the invariant channel-wise relation mask between input features (F_S and F_T) and fused feature map ($Z_{ST} = [Z_{ST}^1, Z_{ST}^2, \dots, Z_{ST}^C]$). Here, we reshape each element (F_S^i and F_T^i) of F_S and F_T to \mathbb{R}^N , where $N = H \times W$. Similarly, we reshape Z_{ST}^i to \mathbb{R}^N . After reshaping, we apply dot product with softmax operation, which is shown in Eq.10 ~ Eq.12.

$$M_S^{j,i} = \frac{\exp(F_S^i \cdot Z_{ST}^j)}{\sum_{i=1}^C (F_S^i \cdot Z_{ST}^j)}, \quad M_T^{j,i} = \frac{\exp(F_T^i \cdot Z_{ST}^j)}{\sum_{i=1}^C (F_T^i \cdot Z_{ST}^j)} \quad (10)$$

$$M_S = \begin{bmatrix} M_S^{1,1} & \dots & M_S^{1,C} \\ \vdots & \ddots & \vdots \\ M_S^{C,1} & \dots & M_S^{C,C} \end{bmatrix} \quad (11)$$

$$M_T = \begin{bmatrix} M_T^{1,1} & \dots & M_T^{1,C} \\ \vdots & \ddots & \vdots \\ M_T^{C,1} & \dots & M_T^{C,C} \end{bmatrix} \quad (12)$$

where $M_S (\mathbb{R}^{C \times C})$ represents the channel-wise relation mask between F_S and Z_{ST} while $M_T (\mathbb{R}^{C \times C})$ represents the channel-wise relation mask between F_T and Z_{ST} . The invariant relation mask is denoted as $M_{ST} = (M_S + M_T)/2$. In M_{ST} , if the value ($M_{ST}^{j,i}$) is larger, it means that the i^{th} channel of F_S and F_T probably both have high impact on the j^{th} channel of M_{ST} .

Since M_{ST} reflects the universal relation, we perform a matrix multiplication between M_{ST} and F_S, F_T to generate features with channel-wise attention. Eq.13 shows this process.

$$F_{I-S}^j = \sum_{i=1}^C (F_S^i \times M_{ST}^{j,i}), \quad F_{I-T}^j = \sum_{i=1}^C (F_T^i \times M_{ST}^{j,i}) \quad (13)$$

where $F_{I-S} = [F_{I-S}^1, F_{I-S}^2, \dots, F_{I-S}^C]$ and $F_{I-T} = [F_{I-T}^1, F_{I-T}^2, \dots, F_{I-T}^C]$ are respectively source-style and target-style invariant features.

Finally, we fuse the unique and invariant feature through concatenation. The outputs of DDM are F'_S and F'_T . The pipeline of DDM is shown in Alg.1.

Algorithm 1 Domain disentangled module

Input: Source-style feature map F_S and target-style feature map F_T extracted from single-domain image. $F_S, F_T \in \mathbb{R}^{C \times H \times W}$. Trainable parameters in fully-connected layers ($f(\cdot), g_S(\cdot), g_T(\cdot)$) and convolutional layers ($f_c(\cdot), f_S(\cdot), f_T(\cdot)$)

Output: New source-style feature map F'_S and target-style feature map F'_T containing unique and invariant information. $F'_S, F'_T \in \mathbb{R}^{C \times H \times W}$.

Feature Fusion:

Get fused prototype z_{ST} using Eq.6.

Get fused feature map Z_{ST} using Eq.6.

Feature Disentangling:
Unique feature disentangling:

Get complementary channel-wise weighted vectors v_S and v_T using Eq.7 and Eq.8.

Get source-style and target-style unique features F_{U-S} and F_{U-T} using Eq.9.

Invariant feature disentangling:

Get channel-wise relation masks M_S and M_T using Eq.10 ~ Eq.12.

Get source-style and target-style invariant features F_{I-S} and F_{I-T} using Eq.13.

Feature concatenation:

Get source-style new features $F'_S = \text{cat}(F_{U-S}, F_{I-S})$.

Get target-style new features $F'_T = \text{cat}(F_{U-T}, F_{I-T})$.

D. Cross-Domain Separated Self-Training Mechanism

From our proposed third and fourth principles in Sec.I, we believe that directly applying adversarial learning mechanism can ease the domain shift, but it will still cause instability and representation tendency on source images. The reason is RS images from different domains have large discrepancy. Motivated by further improving the representation capability

on target images, we propose an EMA based cross-domain separated self-training mechanism. As shown in Fig.4, traditional EMA based self-training paradigm generates a teacher network with EMA updating operation on student network. Compared to traditional paradigm, our self-training paradigm will not generate a whole teacher network, but only generate one or more components. In this paper, we propose two self-training paradigms, which are “Decoder-only” and “Single-target”.

Decoder-only. As shown in Fig.4, “Decoder-only” paradigm introduces two teacher decoders rather than two teacher networks. In this paradigm, student networks get credible and mature knowledge from teacher decoders. Specifically, we first construct two teacher decoders, which are source teacher decoder (H_S^{te}) and target teacher decoder (H_T^{te}). Then, at training step t , the teacher decoders’ weights are updated by student decoders’ weights by exponential moving average (EMA) operation, which can be formulated in Eq.14.

$$\begin{cases} \phi_t^{H_S^{te}} = \alpha \phi_{t-1}^{H_S^{te}} + (1 - \alpha) \theta_t^{H_S} \\ \phi_t^{H_T^{te}} = \alpha \phi_{t-1}^{H_T^{te}} + (1 - \alpha) \theta_t^{H_T} \end{cases} \quad (14)$$

where α denotes the EMA decay factors controlling the updating rate. $\phi_t^{H_S^{te}}, \phi_t^{H_T^{te}}$ refer to weights of two teacher decoders at t^{th} step. $\theta_t^{H_S}, \theta_t^{H_T}$ refer to weights of two student decoders (H_S, H_T) at t^{th} step.

After updating the weights of teacher decoders, we transfer the reliable knowledge to student by pseudo-label guidance. With two teacher decoders, the generation of pseudo-label is formulated in Eq.15.

$$\hat{P}_t^{te} = \arg \max_c \frac{(H_S^{te}(F'_{S-t}) + H_T^{te}(F'_{T-t}))}{2} \quad (15)$$

where $F'_{S-t} \in \mathbb{R}^{C \times H \times W}$ and $F'_{T-t} \in \mathbb{R}^{C \times H \times W}$ are respectively target-domain source-style feature and target-domain target-style feature after DDM (Alg.1). $\hat{P}_t^{te} \in \mathbb{R}^{H \times W}$ is pseudo-label (index map) after channel-wise $\arg \max$ operation. Here, we apply soft-voting ensemble strategy to integrate the predictions after two teacher decoders, which makes the pseudo-label more credible.

“Decoder-only” paradigm has two main advantages. (1) It can efficiently transfer reliable knowledge to both source and target students (including backbone and decoder) for target-style feature extraction, which maximally alleviates the representation tendency on source images. (2) It can efficiently save a lot of training memory and computation cost because decoder of a segmentation network is always much smaller than backbone.

Single-target. In this paper, we propose “Single-target” paradigm, which is another self-training paradigm on our proposed DASegNet. This paradigm mainly aims to enhance the target-style feature representation of target student backbone and decoder. As shown in Fig.4, we construct a whole target teacher network including target teacher backbone (B_T^{te}) and

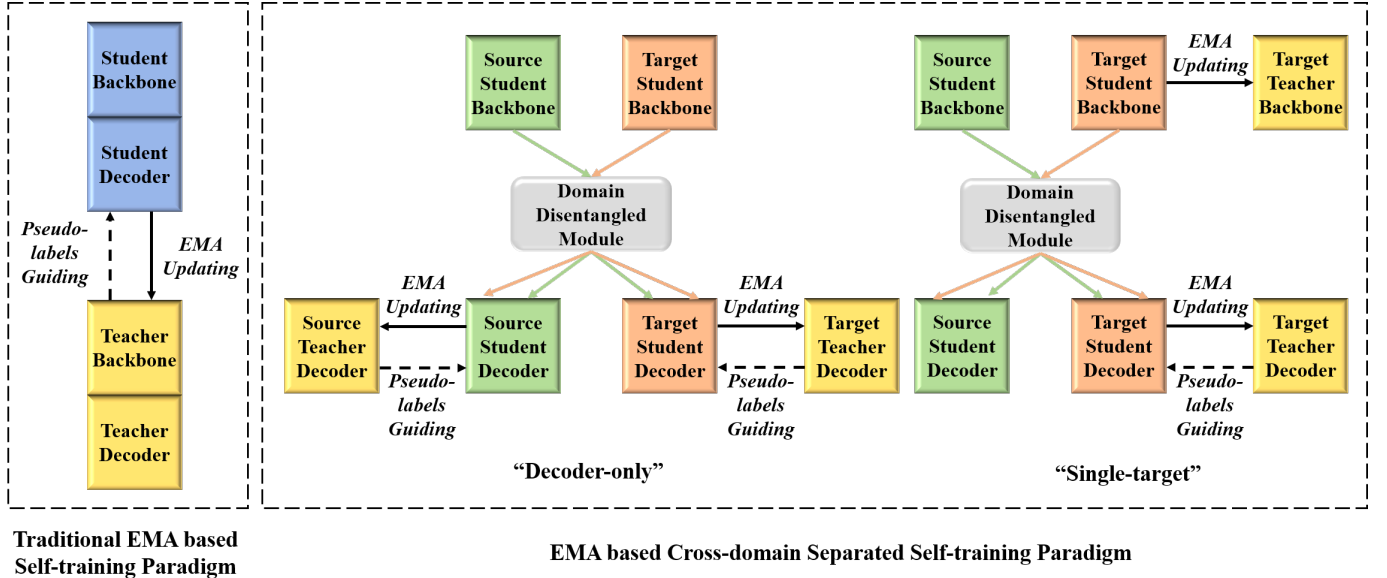


Fig. 4. Comparison between traditional EMA based self-training paradigm and our proposed EMA based cross-domain separated self-training paradigm.

target teacher decoder (H_T^{te}). Similar to Eq.14, we apply EMA updating on target teacher network, which is shown in Eq.16.

$$\begin{cases} \phi_t^{B_T^{te}} = \alpha \phi_{t-1}^{B_T^{te}} + (1 - \alpha) \theta_t^{B_T} \\ \phi_t^{H_T^{te}} = \alpha \phi_{t-1}^{H_T^{te}} + (1 - \alpha) \theta_t^{H_T} \end{cases} \quad (16)$$

where $\phi_t^{B_T^{te}}$ refers to weights of target teacher backbone at t^{th} step. $\theta_t^{B_T}$ refers to weights of target student backbone at t^{th} step.

With a whole teacher networks, the pseudo-label generation of “Single-target” paradigm can be expressed in Eq.17.

$$\hat{P}_t^{te} = \arg \max_c H_T^{te}(\mathbf{F}'_{T-t}) \quad (17)$$

Compared to “Decoder-only” paradigm, the main difference is that “Single-target” only employs pseudo-label guiding on target student. Theoretically, “Single-target” paradigm can enhance the target-style feature extraction power on target student, which leads to larger representation gap between source and student network. In practical experiments, we find that “Decoder-only” paradigm can also enhance the target-style feature extraction power on target student with less memory and training computation cost. Basically, both this two paradigm improve the target-domain adaptation ability of DASegNet by pseudo-label guiding. Since two paradigms both can generate credible pseudo-label, they both can improve the performance of DASegNet.

In summary, we show our proposed cross-domain separated self-training mechanism in Alg.2. In this paper, we mainly adopt “Decoder-only” paradigm. “Single-target” paradigm provides another perspective on integrating self-training mechanism into DASegNet. In experiments, we will make further comparison between these two paradigms.

Algorithm 2 Cross-domain separated self-training mechanism

Input: Target images x_t . Source student backbone B_S , target student backbone B_T , source student decoder H_S and target student decoder H_T .

Output: Trainable parameters of teacher network components at t^{th} step. Pseudo-label \hat{P}_t^{te} .

if Self-training paradigm is “Decoder-only” **then**

EMA Updataing:

Update source teacher decoder H_S^{te} and target teacher decoder H_T^{te} at t^{th} step using Eq.14.

Pseudo-label Generation:

Extract features (\mathbf{F}_{S-t} , \mathbf{F}_{T-t}) on x_t respectively from B_S and B_T using Eq.1 and Eq.2

Get disentangle features (\mathbf{F}'_{S-t} , \mathbf{F}'_{T-t}) from DDM with \mathbf{F}_{S-t} and \mathbf{F}_{T-t} as input using Alg.1.

Get pseudo-label \hat{P}_t^{te} with \mathbf{F}'_{S-t} and \mathbf{F}'_{T-t} as input using Eq.15.

end if

if Self-training paradigm is “Single-target” **then**

EMA Updataing:

Update target teacher backbone B_T^{te} and target teacher decoder H_T^{te} at t^{th} step using Eq.16.

Pseudo-label Generation:

Extract features (\mathbf{F}_{S-t} , \mathbf{F}_{T-t}^{te}) on x_t respectively from B_S and B_T^{te} using Eq.1 and Eq.2.

Get disentangle features (\mathbf{F}'_{S-t} , \mathbf{F}'_{T-t}) from DDM with \mathbf{F}_{S-t} and \mathbf{F}_{T-t}^{te} as input using Alg.1.

Get pseudo-label \hat{P}_t^{te} with \mathbf{F}'_{T-t} as input using Eq.17.

end if

E. Optimization with Combined Loss

In this paper, we apply segmentation loss, adversarial loss and self-training loss to jointly optimize the ST-DASegNet.

As for segmentation loss (\mathcal{L}_{seg}^S and \mathcal{L}_{seg}^T) shown in Fig.2, we apply conventional cross-entropy loss using annotations of

TABLE I
CROSS-DOMAIN RS IMAGE SEMANTIC SEGMENTATION COMPARISON RESULTS (%) FROM POTSDAM IR-R-G TO VAIHINGEN IR-R-G. METHODS WITH
“*” ARE OUR REIMPLEMENTED VERSION.

Methods	Clutter		Impervious surfaces		Car		Tree		Low vegetation		Building		Overall	
	<i>IoU</i>	<i>F1-score</i>	<i>IoU</i>	<i>F1-score</i>	<i>IoU</i>	<i>F1-score</i>	<i>IoU</i>	<i>F1-score</i>	<i>IoU</i>	<i>F1-score</i>	<i>IoU</i>	<i>F1-score</i>	<i>mIoU</i>	<i>mF-score</i>
DeeplabV3 [14] (Baseline)	2.33	4.56	43.90	60.78	24.26	39.07	52.25	64.19	25.76	40.87	60.35	71.81	34.81	46.88
SegFormer [15] (Baseline)	4.22	9.47	61.03	76.07	31.13	47.89	66.31	78.87	44.47	60.38	75.50	87.95	46.11	60.11
AdaptSegNet [17]	4.60	8.76	54.39	70.39	6.40	11.99	52.65	68.96	28.98	44.91	63.14	77.40	35.02	47.05
FSDAN [60]	10.00	-	57.40	-	37.00	-	58.40	-	41.70	-	57.80	-	43.70	-
ProDA [61]	3.99	8.21	62.51	76.85	39.20	56.52	56.26	72.09	34.49	51.65	71.61	82.95	44.68	58.05
DualGAN [51]	29.66	45.65	49.41	66.13	34.34	51.09	57.66	73.14	38.87	55.97	62.30	76.77	45.38	61.43
Bai <i>et al.</i> [56]	19.60	32.80	65.00	78.80	39.60	56.70	54.80	70.80	36.20	53.20	76.00	86.40	48.50	63.10
Zhang <i>et al.</i> [59]	20.71	31.34	67.74	80.13	44.90	61.94	55.03	71.90	47.02	64.16	76.75	86.65	52.03	66.02
ResiDualGAN [55]	11.64	18.42	72.29	83.89	57.01	72.51	63.81	77.88	49.69	66.29	80.57	89.23	55.83	68.04
DAFormer [21]*	48.26	60.17	74.09	84.12	38.96	56.41	70.88	81.36	57.53	71.48	84.07	90.75	62.30	74.05
ST-DASegNet (DeeplabV3)	21.17	32.64	70.88	82.20	51.81	67.63	68.01	80.10	41.97	57.97	82.57	89.24	56.07	68.30
ST-DASegNet (SegFormer)	67.03	80.28	74.43	85.36	43.38	60.49	67.36	80.49	48.57	65.37	85.23	92.03	64.33	77.34

source images. We formulate segmentation loss function in Eq.18 and Eq.19.

$$\mathcal{L}_{seg}^S = - \sum_{h=1}^H \sum_{w=1}^W \sum_{c=1}^C (\mathbf{y}_s(\mathbf{h}, \mathbf{w}, \mathbf{c}) \log(H_S(\mathbf{F}'_{S-s}))) \quad (18)$$

$$\mathcal{L}_{seg}^T = - \sum_{h=1}^H \sum_{w=1}^W \sum_{c=1}^C (\mathbf{y}_s(\mathbf{h}, \mathbf{w}, \mathbf{c}) \log(H_T(\mathbf{F}'_{T-s}))) \quad (19)$$

where, \mathbf{y}_s is the ground truth of source images. \mathbf{F}'_{S-s} and \mathbf{F}'_{T-s} are respectively source-domain source-style and source-domain target-style disentangled features after DDM.

As for self-training loss (\mathcal{L}_{st}^S and \mathcal{L}_{st}^T) shown in Fig.2, we also adopt cross-entropy loss using pseudo-labels of target images. We formulate self-training loss function in Eq.20 and Eq.21.

$$\mathcal{L}_{st}^S = - \sum_{h=1}^H \sum_{w=1}^W \sum_{c=1}^C (\hat{\mathbf{P}}_t^{te}(\mathbf{h}, \mathbf{w}, \mathbf{c}) \log(H_S(\mathbf{F}'_{S-t}))) \quad (20)$$

$$\mathcal{L}_{st}^T = - \sum_{h=1}^H \sum_{w=1}^W \sum_{c=1}^C (\hat{\mathbf{P}}_t^{te}(\mathbf{h}, \mathbf{w}, \mathbf{c}) \log(H_T(\mathbf{F}'_{T-t}))) \quad (21)$$

where, $\hat{\mathbf{P}}_t^{te}$ denotes the pseudo-labels of target images, which is transformed from index maps ($\mathbb{R}^{H \times W}$) to one-hot labels ($\mathbb{R}^{C \times H \times W}$). The calculation operation of $\hat{\mathbf{P}}_t^{te}$ is shown in Eq.15 or Eq.17 respectively for “Decoder-only” and “Single-target” paradigms.

To optimize ST-DASegNet, we combine three types of losses together. The final combined loss function (\mathcal{L}) is formulated in Eq.22.

$$\mathcal{L} = \mathcal{L}_{seg} + \lambda \mathcal{L}_{st} + \beta \mathcal{L}_{adv} \quad (22)$$

where $\mathcal{L}_{seg} = \mathcal{L}_{seg}^S + \mathcal{L}_{seg}^T$ (Eq.18 and Eq.19). $\mathcal{L}_{st} = \mathcal{L}_{st}^S + \mathcal{L}_{st}^T$ (Eq.20 and Eq.21). $\mathcal{L}_{adv} = \mathcal{L}_{adv}^{B_S} + \mathcal{L}_{adv}^{B_T}$ (Eq.3 and Eq.4). λ and β are two factors to adjust the proportion of self-training loss and adversarial loss. In this paper, we set $\lambda = 0.25$ and $\beta = 0.005$.

IV. EXPERIMENTS AND ANALYSIS

A. Datasets and Evaluation Metric

To evaluate our method on cross-domain RS image semantic segmentation task, we use three benchmark datasets, which are Potsdam, Vaihingen and LoveDA.

Potsdam and Vaihingen. These two datasets belong to ISPRS 2D semantic segmentation benchmark dataset [22]. The Potsdam dataset contains 38 VHR TOP (very-high-resolution True Orthophotos) with size of 6000×6000 (fixed size). The Potsdam dataset has three different imaging modes, which are IR-R-G, R-G-B and R-G-B-IR. The first two modes are 3-channel while the last mode is 4-channel. In this paper, we choose to use the first two modes. The Vaihingen dataset contains 33 VHR TOP with size of 2000×2000 (approximate size). The Vaihingen dataset only has one imaging mode, which is IR-R-G. For more efficient computation cost, we crop the images of these two datasets into smaller patches with size of 512×512 . Specifically, we respectively select 512 and 256 as cropping stride for Potsdam and Vaihingen, generating 4598 and 1696 patches. Moreover, we split the Potsdam and Vaihingen datasets into training and testing set. For Potsdam, the training and testing set contain 2904 and 1694 images, respectively. For Vaihingen, the training and testing set contain 1296 and 440 images, respectively. It is worth noting that, all the data preprocessing methods are followed previous works [51], [53], [55], [56], [59].

On Potsdam/Vaihingen datasets, we design four cross-domain RS semantic segmentation tasks, which are listed as follows.

- Potsdam IR-R-G to Vaihingen IR-R-G (Potsdam IR-R-G \rightarrow Vaihingen IR-R-G).
- Vaihingen IR-R-G to Potsdam IR-R-G (Vaihingen IR-R-G \rightarrow Potsdam IR-R-G).
- Potsdam R-G-B to Vaihingen IR-R-G (Potsdam R-G-B \rightarrow Vaihingen IR-R-G).
- Vaihingen IR-R-G to Potsdam R-G-B (Vaihingen IR-R-G \rightarrow Potsdam R-G-B).

LoveDA. This dataset is recently proposed to advance both RS semantic segmentation and domain adaptation tasks. It

TABLE II
CROSS-DOMAIN RS IMAGE SEMANTIC SEGMENTATION COMPARISON RESULTS (%) FROM VAIHINGEN IR-R-G TO POTSDAM IR-R-G. METHODS WITH “*” ARE OUR REIMPLEMENTED VERSION.

Methods	Clutter		Impervious surfaces		Car		Tree		Low vegetation		Building		Overall	
	<i>IoU</i>	<i>F1-score</i>	<i>IoU</i>	<i>F1-score</i>	<i>IoU</i>	<i>F1-score</i>	<i>IoU</i>	<i>F1-score</i>	<i>IoU</i>	<i>F1-score</i>	<i>IoU</i>	<i>F1-score</i>	<i>mIoU</i>	<i>mF-score</i>
DeeplabV3 [14] (Baseline)	5.28	11.58	55.57	71.07	50.02	66.97	14.0	27.69	43.67	60.70	60.62	75.02	38.19	52.17
SegFormer [15] (Baseline)	1.08	2.65	60.63	76.47	58.99	73.14	30.07	46.24	51.91	68.82	74.85	87.18	46.29	59.08
AdaptSegNet [17]	8.36	15.33	49.55	64.64	40.95	58.11	22.59	36.79	34.43	61.50	48.01	63.41	33.98	49.96
ProDA [61]	10.63	19.21	44.70	61.72	46.78	63.74	31.59	48.02	40.55	57.71	56.85	72.49	38.51	53.82
DualGAN [51]	11.48	20.56	51.01	67.53	48.49	65.31	34.98	51.82	36.50	53.48	53.37	69.59	39.30	54.71
Zhang <i>et al.</i> [59]	12.31	24.59	64.39	78.59	59.35	75.08	37.55	54.60	47.17	63.27	66.44	79.84	47.87	62.66
DAFormer [21]*	2.56	5.02	68.42	79.07	65.20	79.31	70.65	82.13	56.39	72.48	78.94	87.64	57.03	67.61
ST-DASegNet (DeeplabV3)	5.21	10.21	74.19	85.26	76.76	86.90	43.33	60.44	51.56	68.62	82.15	90.28	55.53	66.95
ST-DASegNet (SegFormer)	0.18	0.35	76.45	86.65	73.54	84.76	62.89	77.22	61.04	75.80	83.81	91.19	59.65	69.33

consists of 5987 high spatial resolution (1024×1024) RS images from three cities including Nanjing, Changzhou, and Wuhan. LoveDA dataset contains images from two domains (urban and rural), which focus on challenging the model’s generalized representation capacity on different geographical elements of urban and rural scenes. This dataset has 1833 urban images, which is split into 1156 training images and 677 validation images. For rural images, there are 2358 images in total, where 1366 images are used for training and the rest 992 images are used for validation. In addition, LoveDA also contains 1796 testing images (976 for rural and 820 for urban), which can be evaluated on online server¹. On LoveDA dataset, we design two cross-domain RS semantic segmentation tasks, which are urban-to-rural (urban \rightarrow rural) and rural-to-urban (rural \rightarrow urban) task. All our experiments setting are followed [23], [57].

Evaluation Metric. In this paper, we select common-used *IoU* (intersection of union) and *F1-score* as evaluation metrics. Specifically, for a specific class i , *IoU* is formulated as $IoU_i = tp_i / (tp_i + fp_i + fn_i)$, where tp_i , fp_i , fn_i denote true positive, false positive and false negative, respectively. The *mIoU* is the mean value of all the IoU_i . Additionally, *F1-score* is defined as $F1\text{-score} = (2 \times Precision \times Recall) / (Precision + Recall)$.

B. Implementation Details

Followed previous works, we select DeeplabV3 [14] as baseline segmentation network. We also select recent outstanding segmentation network, SegFormer [15] as another baseline. If applying DeeplabV3, the student backbone will be ResNet-50 [62] and the student decoder will be ASPP block (a combination of ASPP module and several convolutional blocks). To optimize DeeplabV3 based ST-DASegNet, we use SGD (Stochastic Gradient Descent) as optimizer, where the initial learning rate is 0.001, momentum value is 0.9 and weight decay value is 0.0001. If applying SegFormer, the student backbone will be mit-b5 and the student decoder will be “All MLP” module. To optimize SegFormer based ST-DASegNet, we use Adam as optimizer and the initial learning rate is set as 0.0001.

For DeeplabV3 and SegFormer based ST-DASegNet, we both apply Adam as optimizer in which the initial learning rate is 0.00025. The structure of our proposed discriminators (D_S and D_T) is followed PatchGAN [63]. Specifically, the discriminator consists of 4 convolutional blocks with kernels as size of 4×4 . The stride of the first two and the last two blocks is respectively set as 2 and 1. The output channels of each block are 64, 128, 256, 1.

All experiments are implemented on mmsegmentation² semantic segmentation framework and all models are trained on two NVIDIA RTX 3090. Our code is available at <https://github.com/cv516Buaa/ST-DASegNet>.

C. Experimental Results

1) *Cross-domain RS image semantic segmentation on Potsdam and Vaihingen:* As mentioned above, we design four cross-domain tasks between Potsdam and Vaihingen. On this four tasks, we conduct abundant experiments to show the effectiveness of our proposed ST-DASegNet. Previous methods always select DeeplabV3 as baseline model and hardly apply transformer as baseline model. Therefore, we reimplement DAFormer [21] to fairly compare with our SegFormer based ST-DASegNet. It is worth noting that DAFormer [21] is the first method applying transformer (SegFormer) on cross-domain natural scene image semantic segmentation task. Similar to our method, DAFormer also uses mmsegmentation to implement their method, so we can easily apply DAFormer on cross-domain RS image semantic segmentation task.

Comparison experiments from Potsdam IR-R-G to Vaihingen IR-R-G. In this task, Potsdam IR-R-G and Vaihingen IR-R-G images are respectively served as source-domain and target-domain. The 2904 annotated training images from Potsdam and 1296 no-annotation training images from Vaihingen are used to train the model. The 440 Vaihingen testing images are used for evaluation. The comparison results are shown in Tab.I. Compared to DeeplabV3 based methods, ST-DASegNet (DeeplabV3) surpasses the current SOTA method [55]. Compared to SegFormer based method (DAFormer [21]), ST-DASegNet (SegFormer) achieves 2.03% improvement on *mIoU* value and 3.29% improvement on

¹<https://github.com/Junjue-Wang/LoveDA>

²<https://github.com/open-mmlab/msegmentation>

TABLE III
CROSS-DOMAIN RS IMAGE SEMANTIC SEGMENTATION COMPARISON RESULTS (%) FROM POTSDAM R-G-B TO VAIHINGEN IR-R-G. METHODS WITH “*” ARE OUR REIMPLEMENTED VERSION.

Methods	Clutter		Impervious surfaces		Car		Tree		Low vegetation		Building		Overall	
	<i>IoU</i>	<i>F1-score</i>	<i>IoU</i>	<i>F1-score</i>	<i>IoU</i>	<i>F1-score</i>	<i>IoU</i>	<i>F1-score</i>	<i>IoU</i>	<i>F1-score</i>	<i>IoU</i>	<i>F1-score</i>	<i>mIoU</i>	<i>mF-score</i>
DeeplabV3 [14] (Baseline)	0.58	1.16	40.42	57.57	12.52	22.25	30.88	47.19	12.12	21.62	54.23	70.33	25.12	36.68
SegFormer [15] (Baseline)	1.43	2.81	51.34	67.85	37.97	55.04	52.62	68.96	5.18	9.85	73.18	84.51	36.95	48.17
AdaptSegNet [17]	2.99	5.81	51.26	67.77	10.25	18.54	51.51	68.02	12.75	22.61	60.72	75.55	31.58	43.05
ProDA [61]	2.39	5.09	49.04	66.11	31.56	48.16	49.11	65.86	32.44	49.06	68.94	81.89	38.91	52.70
DualGAN [51]	3.94	13.88	49.16	61.33	40.31	57.88	55.82	70.66	27.85	42.17	65.44	83.00	39.93	54.82
Bai <i>et al.</i> [56]	10.80	19.40	62.40	76.90	38.90	56.00	53.90	70.00	35.10	51.90	74.80	85.60	46.00	60.00
Zhang <i>et al.</i> [59]	12.38	21.55	64.47	77.76	43.43	60.05	52.83	69.62	38.37	55.94	76.87	86.95	48.06	61.98
ResiDualGAN [55]	9.76	16.08	55.54	71.36	48.49	65.19	57.79	73.21	29.15	44.97	78.97	88.23	46.62	59.84
DAFormer [21]*	22.57	33.72	67.44	79.65	45.60	60.13	66.27	80.41	40.49	54.93	81.34	90.07	53.95	66.49
ST-DASegNet (DeeplabV3)	20.53	33.74	62.60	76.39	47.32	64.30	61.71	74.89	29.72	44.43	75.58	86.13	49.58	63.31
ST-DASegNet (SegFormer)	36.03	50.64	68.36	81.28	43.15	60.28	64.65	78.31	34.69	47.08	84.09	91.33	55.16	68.15

TABLE IV
CROSS-DOMAIN RS IMAGE SEMANTIC SEGMENTATION COMPARISON RESULTS (%) FROM VAIHINGEN IR-R-G TO POTSDAM R-G-B. METHODS WITH “*” ARE OUR REIMPLEMENTED VERSION.

Methods	Clutter		Impervious surfaces		Car		Tree		Low vegetation		Building		Overall	
	<i>IoU</i>	<i>F1-score</i>	<i>IoU</i>	<i>F1-score</i>	<i>IoU</i>	<i>F1-score</i>	<i>IoU</i>	<i>F1-score</i>	<i>IoU</i>	<i>F1-score</i>	<i>IoU</i>	<i>F1-score</i>	<i>mIoU</i>	<i>mF-score</i>
DeeplabV3 [14] (Baseline)	4.61	8.82	46.02	63.03	59.71	74.77	1.63	3.53	7.1	13.25	37.34	54.37	26.07	36.30
SegFormer [15] (Baseline)	2.36	4.61	62.45	76.89	72.16	83.83	5.38	10.21	31.52	48.65	72.61	84.13	41.08	51.39
AdaptSegNet [17]	6.11	11.50	37.66	59.55	42.31	55.95	30.71	45.51	15.10	25.81	54.25	70.31	31.02	44.75
ProDA [61]	11.13	20.51	44.77	62.03	41.21	59.27	30.56	46.91	35.84	52.75	46.37	63.06	34.98	50.76
DualGAN [51]	13.56	23.84	45.96	62.97	39.71	56.84	25.80	40.97	41.73	58.87	59.01	74.22	37.63	52.95
Zhang <i>et al.</i> [59]	13.27	23.43	57.65	73.14	56.99	72.27	35.87	52.80	29.77	45.88	65.44	79.11	43.17	57.77
DAFormer [21]*	1.07	1.88	65.12	78.16	70.40	84.28	61.25	76.59	49.02	65.51	82.44	89.70	54.88	66.02
ST-DASegNet (DeeplabV3)	2.66	4.29	65.48	79.27	75.15	85.86	34.46	47.95	45.59	63.13	78.06	87.66	50.23	61.36
ST-DASegNet (SegFormer)	3.70	7.38	69.83	83.12	75.99	87.89	57.41	73.47	50.76	67.64	83.46	90.67	56.86	68.37

mF-score. From Tab.I, we also find that even though the baseline model performs strong, ST-DASegNet (SegFormer) can still gain 20.22% improvement on *mIoU* value and 17.23% improvement on *mF*-score. Particularly, on “Clutter” category, ST-DASegNet (SegFormer) shows outstanding performance over previous methods. On this single category, ST-DASegNet surpasses the second best method (DAFormer) by 18.77% on *IoU* value and 20.11% on *F1*-score.

Comparison experiments from Vaihingen IR-R-G to Potsdam IR-R-G. In this task, Vaihingen IR-R-G and Potsdam IR-R-G images are respectively served as source-domain and target-domain. The 1296 annotated training images from Vaihingen and 2904 no-annotation training images from Potsdam are used to train the model. The 1694 Potsdam testing images are used for evaluation. As shown in Tab.II, DeeplabV3 based ST-DASegNet performs much stronger than previous methods. Compared to previous SOTA method [59], it achieves 7.66% improvement on *mIoU* value and 4.29% on *mF*-score. SegFormer based ST-DASegNet also shows obvious superiority over DAFormer.

Comparison experiments from Potsdam R-G-B to Vaihingen IR-R-G. In this task, Potsdam R-G-B and Vaihingen IR-R-G images are respectively served as source-domain and target-domain. The 2904 annotated training images from Potsdam and 1296 no-annotation training images from Vaihingen

are used to train the model. The 440 Vaihingen testing images are used for evaluation. As shown in Fig.1, “Potsdam R-G-B to Vaihingen IR-R-G” adaptation is more complex than “Potsdam IR-R-G to Vaihingen IR-R-G” adaptation. Besides suffering from different ground sampling distance, this task also suffers from remote sensing sensor variation. The comparison results on this task are shown in Tab.III. Obviously, DeeplabV3 and SegFormer based ST-DASegNet respectively outperform Zhang *et al.* [59] and DAFormer [21] and achieve SOTA results. In addition, Similar to the results on “Potsdam R-G-B to Vaihingen IR-R-G” task, ST-DASegNet also outperforms second best method by large margin on “Clutter” category.

Comparison experiments from Vaihingen IR-R-G to Potsdam R-G-B. In this task, Vaihingen IR-R-G and Potsdam R-G-B images are respectively served as source-domain and target-domain. The 1296 annotated training images from Vaihingen and 2904 no-annotation training images from Potsdam are used to train the model. The 1694 Potsdam testing images are used for evaluation. From Tab.IV, we also obtain encouraging results. On this task, DeeplabV3 based ST-DASegNet shows surprising improvement. Compared to baseline results, it gains 24.16% on *mIoU* value and 25.06% on *mF*-score. Compared to recent best DeeplabV3 based method [59], it leads by 7.06% on *mIoU* value and 3.59% on *mF*-score. Moreover, SegFormer based ST-DASegNet achieves best per-

TABLE V

CROSS-DOMAIN RS IMAGE SEMANTIC SEGMENTATION COMPARISON RESULTS (%) FROM RURAL TO URBAN OF LOVE-DA TEST DATASET. METHODS WITH “*” ARE OUR REIMPLEMENTED VERSION. “AT” INDICATES ADVERSARIAL TRAINING AND “ST” INDICATES SELF-TRAINING.

Methods	Type	<i>IoU</i>							<i>mIoU</i>
		Background	Building	Road	Water	Barren	Forest	Agriculture	
DeeplabV3 [14] (Baseline)	-	32.81	43.41	27.59	79.23	14.84	29.24	20.97	35.44
SegFormer [15] (Baseline)	-	44.98	43.93	27.46	85.82	16.24	37.02	30.48	40.85
DDC [64]	-	43.60	15.37	11.98	79.07	14.13	33.08	23.47	31.53
AdaptSegNet [17]	AT	42.35	23.73	15.61	81.95	13.62	28.70	22.05	32.68
FADA [65]	AT	43.89	12.62	12.76	80.37	12.70	32.76	24.79	31.41
CLAN [66]	AT	43.41	25.42	13.75	79.25	13.71	30.44	25.80	33.11
TransNorm [67]	AT	38.37	5.04	3.75	80.83	14.19	33.99	17.91	27.73
PyCDA [68]	ST	38.04	35.86	45.51	74.87	7.71	40.39	11.39	36.25
CBST [69]	ST	48.37	46.10	35.79	80.05	19.18	29.69	30.05	41.32
IAST [70]	ST	48.57	31.51	28.73	86.01	20.29	31.77	36.50	40.48
DCA [57]	ST	45.82	49.60	51.65	80.88	16.70	42.93	36.92	46.36
DAFormer [21]*	ST	50.94	56.66	62.83	89.41	11.99	45.81	25.26	48.99
ST-DASegNet (DeeplabV3)	AT+ST	49.68	51.62	52.41	74.76	10.69	35.67	35.79	44.38
ST-DASegNet (SegFormer)	AT+ST	51.01	54.23	60.52	87.31	15.18	47.43	36.26	50.28

TABLE VI

CROSS-DOMAIN RS IMAGE SEMANTIC SEGMENTATION COMPARISON RESULTS (%) FROM URBAN TO RURAL OF LOVE-DA TEST DATASET. METHODS WITH “*” ARE OUR REIMPLEMENTED VERSION. “AT” INDICATES ADVERSARIAL TRAINING AND “ST” INDICATES SELF-TRAINING.

Methods	Type	<i>IoU</i>							<i>mIoU</i>
		Background	Building	Road	Water	Barren	Forest	Agriculture	
DeeplabV3 [14] (Baseline)	-	26.64	48.14	23.37	43.97	11.35	32.47	50.61	33.79
SegFormer [15] (Baseline)	-	26.60	55.80	35.62	65.44	17.13	40.13	39.65	40.05
DDC [64]	-	25.61	44.27	31.28	44.78	13.74	33.83	25.98	31.36
AdaptSegNet [17]	AT	26.89	40.53	30.65	50.09	16.97	32.51	28.25	32.27
FADA [65]	AT	24.39	32.97	25.61	47.59	15.34	34.35	20.29	28.65
CLAN [66]	AT	22.93	44.78	25.99	46.81	10.54	37.21	24.45	30.39
TransNorm [67]	AT	19.39	36.30	22.04	36.68	14.00	40.62	3.30	24.62
PyCDA [68]	ST	12.36	38.11	20.45	57.16	18.32	36.71	41.90	32.14
CBST [69]	ST	25.06	44.02	23.79	50.48	8.33	39.16	49.65	34.36
IAST [70]	ST	29.97	49.48	28.29	64.49	2.13	33.36	61.37	38.44
DCA [57]	ST	36.38	55.89	40.46	62.03	22.01	38.92	60.52	45.17
DAFormer [21]*	ST	37.39	52.84	41.99	72.05	11.46	46.79	61.27	46.25
ST-DASegNet (DeeplabV3)	AT+ST	33.79	55.95	39.69	69.28	14.19	44.79	62.16	45.69
ST-DASegNet (SegFormer)	AT+ST	36.78	59.83	43.77	73.83	19.38	49.96	67.01	50.08

formance on 4 categories (Impervious surfaces, Car, Low vegetation and building) and achieves the current SOTA results on *mIoU* value and *mF*-score.

2) *Cross-domain RS image semantic segmentation on LoveDA*: Besides cross-domain adaptation between Potsdam and Vaihingen dataset, we further conduct comparison experiments on LoveDA dataset. Tab.V and Tab.VI shows the rural-to-urban and urban-to-rural results, respectively. From the results, we analyze in the following aspects. (1) Compared to previous methods, our method provides an insight on integrating self-training and adversarial training to tackle cross-domain remote sensing image semantic segmentation task. (2) Compared to baseline models, ST-DASegNet makes huge progress. On rural-to-urban adaptation task, ST-DASegNet (DeepLabV3) and ST-DASegNet (SegFormer) respectively surpass the baseline models by 8.94% and 9.43% on *mIoU* value. On urban-to-rural adaptation task, ST-DASegNet (DeepLabV3) and ST-DASegNet (SegFormer) respectively surpass the baseline models by 11.90% and 10.03% on *mIoU*

value. (3) Compared to previous published SOTA methods, DCA [57], our proposed DeepLabV3 based ST-DASegNet achieves comparable results. It has 1.98% inferiority on rural-to-urban adaptation task and 0.52% superiority on urban-to-rural adaptation task. Our proposed SegFormer based ST-DASegNet outperforms DCA by large margin on both these two tasks. (4) For fair comparison with ST-DASegNet (SegFormer), we reimplement DAFormer. It is clear that ST-DASegNet (SegFormer) achieves better results. (5) These two tasks are online competitions. The track is “LoveDA Unsupervised Domain Adaptation Challenge”. Among all the submitted results on rural-to-urban and urban-to-rural adaptation tasks, our method respectively rank 4th and 2nd place. Among published methods, our method achieves new SOTA results, which is encouraging and persuasive.

D. Ablation Study

To separately show the performance of each component, we conduct ablation experiments on “Potsdam IR-R-G to

TABLE VII
ABLATION COMPARISON EXPERIMENTS ON “POTSDAM IR-R-G TO VAIHINGEN IR-R-G” ADAPTATION TASK (%). “ADV” INDICATES ADVERSARIAL LEARNING. “ST” INDICATES SELF-TRAINING.

Methods	Clutter		Impervious surfaces		Car		Tree		Low vegetation		Building		Overall	
	<i>IoU</i>	<i>F1-score</i>	<i>IoU</i>	<i>F1-score</i>	<i>IoU</i>	<i>F1-score</i>	<i>IoU</i>	<i>F1-score</i>	<i>IoU</i>	<i>F1-score</i>	<i>IoU</i>	<i>F1-score</i>	<i>mIoU</i>	<i>mF-score</i>
DeeplabV3 [14] (Baseline)	2.33	4.56	43.90	60.78	24.26	39.07	52.25	64.19	25.76	40.87	60.35	71.81	34.81	46.88
Dual path baseline model	4.14	7.83	44.18	60.09	28.72	42.97	50.60	63.26	27.80	41.35	56.03	68.52	35.26	47.34
+ DDM	6.02	13.72	58.10	72.67	18.62	33.28	54.90	70.04	38.80	56.08	66.05	77.70	40.42	53.92
+ DDM + Adv	16.86	32.77	62.70	76.44	31.51	47.29	74.48	85.32	50.19	67.02	73.56	84.81	51.55	65.61
+ DDM + Adv + ST	21.17	32.64	70.88	82.20	51.81	67.63	68.01	80.10	41.97	57.97	82.57	89.24	56.07	68.30
with Single-target	25.91	38.16	68.57	81.47	49.11	64.17	67.93	80.91	42.08	58.50	80.47	88.71	55.68	68.65
SegFormer [15] (Baseline)	4.22	9.47	61.03	76.07	31.13	47.89	66.31	78.87	44.47	60.38	75.50	87.95	46.11	60.11
Dual path baseline model	5.91	12.16	62.32	76.03	26.39	40.83	67.31	81.23	46.69	63.49	72.88	86.98	46.92	60.55
+ DDM	27.53	44.01	61.61	73.46	36.98	54.05	63.46	74.70	47.17	62.75	79.74	88.73	52.75	66.28
+ DDM + Adv	46.49	63.49	73.1	84.46	41.6	58.77	61.14	75.88	37.45	54.46	84.94	91.86	57.45	71.49
+ DDM + Adv + ST	67.03	80.28	74.43	85.36	43.38	60.49	67.36	80.49	48.57	65.37	85.23	92.03	64.33	77.34
with Single-target	75.24	85.84	73.28	84.57	49.35	66.10	66.54	79.90	50.20	66.79	86.72	92.89	66.89	79.35

TABLE VIII
ABLATION COMPARISON EXPERIMENTS ON “POTSDAM R-G-B TO VAIHINGEN IR-R-G” ADAPTATION TASK (%). “ADV” INDICATES ADVERSARIAL LEARNING. “ST” INDICATES SELF-TRAINING.

Methods	Clutter		Impervious surfaces		Car		Tree		Low vegetation		Building		Overall	
	<i>IoU</i>	<i>F1-score</i>	<i>IoU</i>	<i>F1-score</i>	<i>IoU</i>	<i>F1-score</i>	<i>IoU</i>	<i>F1-score</i>	<i>IoU</i>	<i>F1-score</i>	<i>IoU</i>	<i>F1-score</i>	<i>mIoU</i>	<i>mF-score</i>
DeeplabV3 [14] (Baseline)	0.58	1.16	40.42	57.57	12.52	22.25	30.88	47.19	12.12	21.62	54.23	70.33	25.12	36.68
Dual path baseline model	0.32	0.91	43.27	58.99	18.36	34.58	25.42	43.30	14.75	24.83	51.04	66.16	25.53	38.13
+ DDM	2.80	5.44	50.72	67.30	18.42	31.11	54.34	70.42	21.34	35.18	50.35	66.98	32.99	46.07
+ DDM + Adv	11.92	23.76	53.95	68.00	42.20	59.33	63.37	77.57	20.99	31.88	65.18	77.50	42.94	56.34
+ DDM + Adv + ST	20.53	33.74	62.60	76.39	47.32	64.30	61.71	74.89	29.72	44.43	75.58	86.13	49.58	63.31
with Single-target	24.71	36.53	61.10	76.33	46.53	63.81	57.25	72.70	30.16	45.04	73.25	85.83	48.83	63.37
SegFormer [15] (Baseline)	1.43	2.81	51.34	67.85	37.97	55.04	52.62	68.96	5.18	9.85	73.18	84.51	36.95	48.17
Dual path baseline model	2.92	5.17	53.84	69.20	37.15	55.28	53.91	69.48	5.64	9.33	71.89	83.10	37.56	48.59
+ DDM	13.42	27.26	55.22	71.13	37.33	54.37	53.71	69.86	10.65	19.20	78.86	88.18	41.53	55.00
+ DDM + Adv	21.14	35.27	65.62	79.25	40.53	57.16	60.82	72.91	34.39	51.70	78.35	87.86	50.14	64.03
+ DDM + Adv + ST	36.03	50.64	68.36	81.28	43.15	60.28	64.65	78.31	34.69	47.08	84.09	91.33	55.16	68.15
with Single-target	35.91	51.16	64.57	78.47	45.11	62.17	67.93	80.91	32.08	48.58	80.47	89.31	54.35	68.43

Vaihingen IR-R-G” and “Potsdam R-G-B to Vaihingen IR-R-G” adaptation tasks shown in Tab.VII and Tab.VIII.

1) *Effectiveness of DDM*: Before evaluating the performance of DDM, we first construct a dual path baseline model, because DDM is based on this kind of dual-path structure. This baseline model contains two student backbones and two student decoders. To form it, we simply remove DDM, discriminators and teacher network from ST-DASegNet. Compared to baseline model, it simply adds one more student network. During training, source and target images will respectively pass through two networks and generate four features. During inference, two target predictions from source and target decoders will be integrated with soft voting strategy. Tab.VII and Tab.VIII shows that dual path baseline model has limited improvement compared to baseline model. This little improvement may come from model ensemble strategy in inference phase.

Based on dual path baseline model, we can easily insert DDM and evaluate its performance. As shown in Tab.VII and Tab.VIII, when adding DDM, the performance of new models makes huge progress, which means that the feature fusion and disentangling mechanism enhances the capability of source and target student backbone to extract different style features

on different domain images. With DDM, source and target student backbone can respectively represent the target images into source-style and target-style with only source annotations.

2) *Effectiveness of feature-level adversarial learning*: After inserting DDM into the model, we further apply feature-level adversarial learning. From Tab.VII and Tab.VIII, it is obvious that the performance of models is skyrocketing. DeepLabv3 based models improve by average 10.54% on *mIoU* value and 10.98% on *mF-score* on “Potsdam IR-R-G to Vaihingen IR-R-G” and “Potsdam R-R-B to Vaihingen IR-R-G” adaptation tasks. SegFormer based models improve by 6.66% on *mIoU* value and 7.12% on *mF-score* on the two tasks. These encouraging results demonstrate that feature-level adversarial learning can ease the domain shift problem by aligning single-style features from different domain images. Moreover, these results also prove the effectiveness of applying feature-level adversarial learning on DDM based model.

3) *Effectiveness of EMA based cross-domain separated self-training mechanism*: Based on DDM and adversarial learning, we add EMA based cross-domain separated self-training mechanism into the model and form the final ST-DASegNet. As shown in Tab.VII and Tab.VIII, with our proposed self-training mechanism, the performance get further improved.

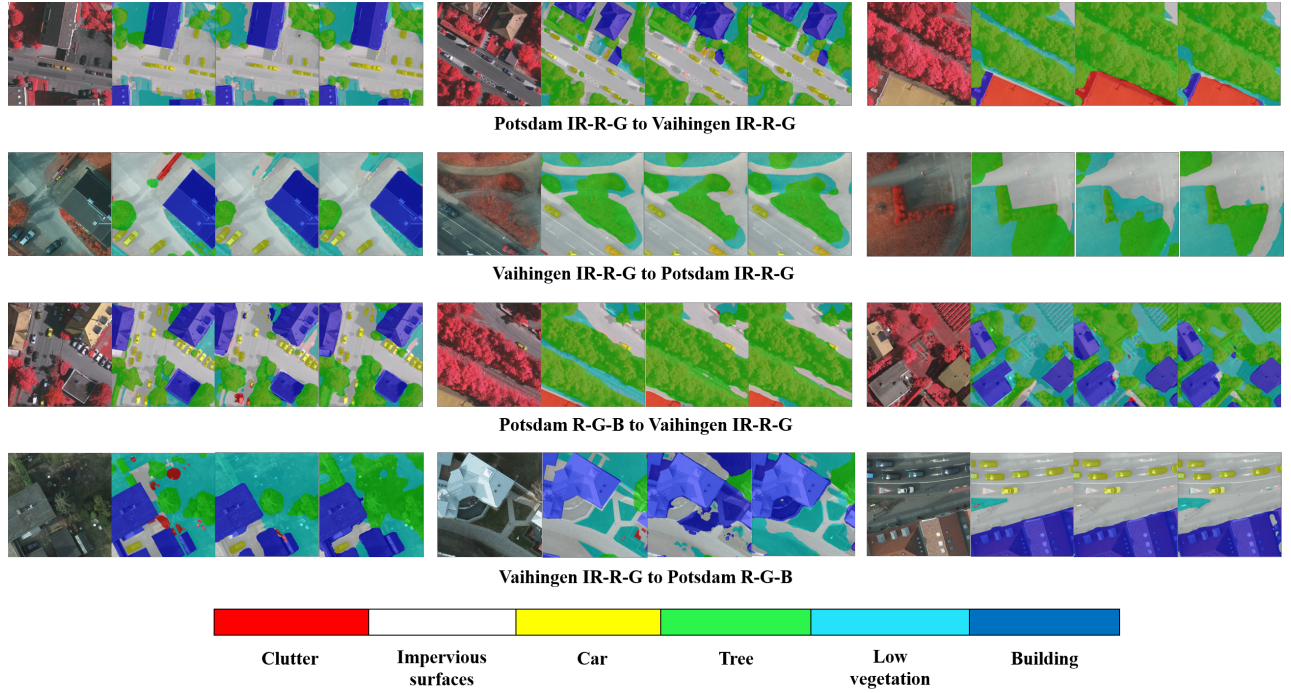


Fig. 5. Qualitative visualization of results on Potsdam and Vaihingen datasets. For each task, we provide 3 cases containing 4 images. From left to right, the 4 images are respectively target images, ground truth, prediction of ST-DASegNet (DeepLabV3) and prediction of ST-DASegNet (SegFormer).

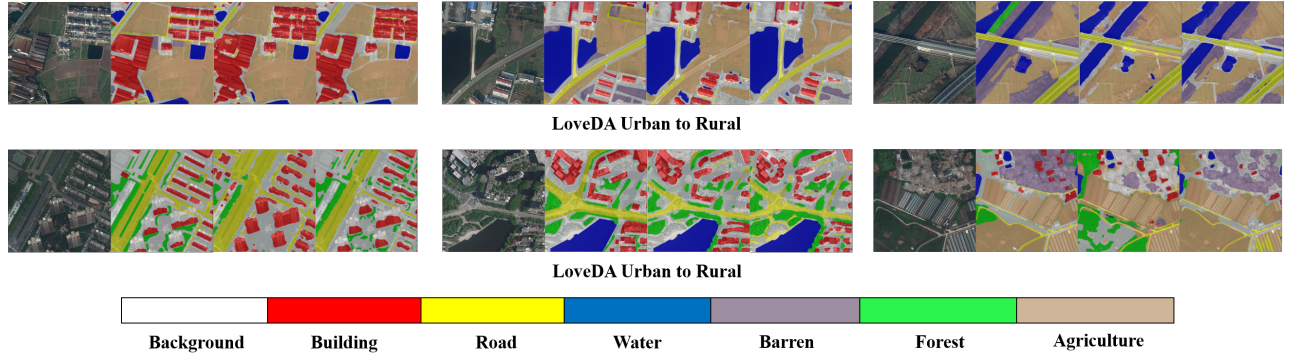


Fig. 6. Qualitative visualization of results on LoveDA datasets. For each task, we provide 3 cases containing 4 images. From left to right, the 4 images are respectively target images, ground truth, prediction of ST-DASegNet (DeepLabV3) and prediction of ST-DASegNet (SegFormer).

From these results, it is clear that the models benefit from high-quality pseudo-labels, which suppresses the representation tendency on source annotated images. The results also show that our proposed self-training mechanism can efficiently incorporate with DDM and adversarial learning.

4) “Decoder-only” Versus “Single-target”: In this paper, we propose two self-training paradigms. To compare their performance, we conduct experiments in Tab.VII and Tab.VIII. On “Potsdam IR-R-G to Vaihingen IR-R-G” task, ST-DASegNet (SegFormer) with “Single-target” paradigm outperforms ST-DASegNet (SegFormer) with “Decoder-only” paradigm by 2.56% on $mIoU$ value and 2.01% on mF -score. ST-DASegNet (DeepLabV3) achieves comparable results with these two paradigms. From the results on “Potsdam R-G-B to Vaihingen IR-R-G” task, “Single-target” paradigm has little inferiority compared to “Decoder-only” paradigm. Generally,

“Single-target” and “Decoder-only” have close performance. Due to less training computation cost, we mainly adopt “Decoder-only” in this paper. Despite that “Single-target” can not beat “Decoder-only”, it still provides an another inspiring paradigm for EMA based cross-domain separated self-training mechanism.

All in all, DDM is designed to improve the model by enhancing feature representation capacity. Feature-level adversarial learning is mainly used to ease the domain-shift problem. EMA based cross-domain separated self-training mechanism makes effect on balance the representation tendency between source and target domain images. This three key components of ST-DASegNet show great compatibility, which can improve the model from three different perspectives.

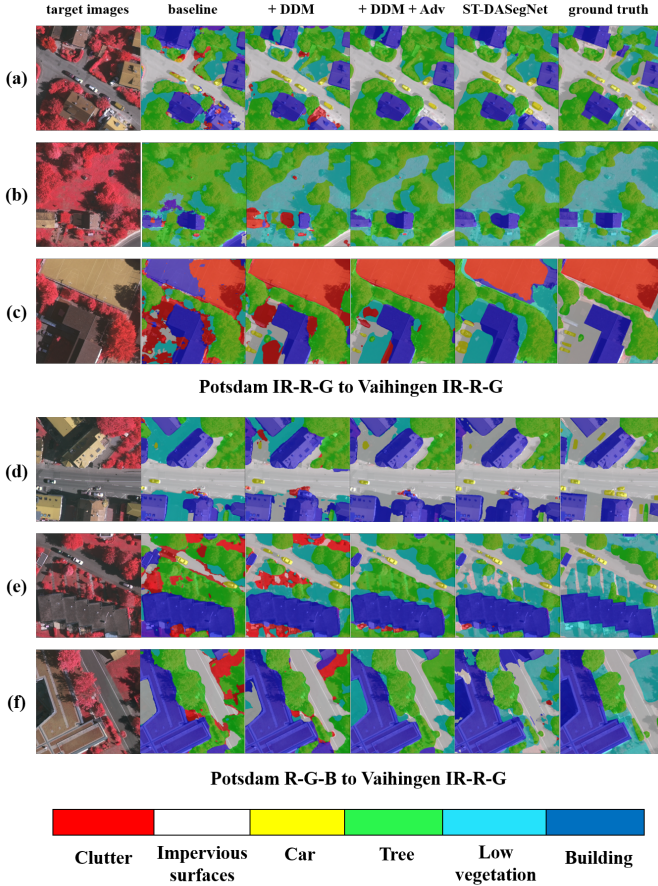


Fig. 7. ablation visualization on “Potsdam IR-R-G to Vaihingen IR-R-G” task (Tab.VII) and “Potsdam R-G-B to Vaihingen IR-R-G” task (Tab.VIII). For each task, we provide 3 cases containing 6 images. From left to right, the first images are target images. The rest 5 images are respectively predictions of baseline model, model with DDM, model with DDM and adversarial learning mechanism, model with DDM, adversarial learning mechanism and self-training mechanism (ST-DASegNet), ground truth. Here, we select SegFormer as baseline model. Particularly, we do not provide results of dual path baseline model, because it achieves comparable performance as baseline model and does not contain any key component.

E. Visualization and Analysis

1) *Qualitative visualization of segmentation results:* From Tab.I to Tab.VI, we report the experimental results of our proposed ST-DASegNet on 6 cross-domain RS image semantic segmentation tasks. Here, we visualize the predictions using above-mentioned trained models to intuitively show the improvement of ST-DASegNet.

As shown in Fig.5, we can intuitively find that ST-DASegNet has strong performance on cross-domain RS image semantic segmentation task between Potsdam and Vaihingen datasets. Specifically, from the most right case on “Potsdam IR-R-G to Vaihingen IR-R-G” task, we find ST-DASegNet has excellent perceptual ability on “Clutter” category, which coincides with the results shown in Tab.I. From the middle and the most right cases on “Vaihingen IR-R-G to Potsdam IR-R-G” task, ST-DASegNet shows strong ability on distinguishing “Tree” and “Low vegetation”. Similar results appear in Tab.II, where results of “Tree” and “Low vegetation”

categories improve by large margin compared to baseline results. On “Potsdam R-G-B to Vaihingen IR-R-G” task, The 3 visualization cases further confirm the results in Tab.III, where ST-DASegNet makes huge progress on segmenting “Clutter”, “Impervious surfaces” and “Building” categories. On “Potsdam R-G-B to Vaihingen IR-R-G” task, the most right case shows the outstanding performance on recognizing “Car”. As shown in Tab.IV, both ST-DASegNet (DeeplabV3) and ST-DASegNet (SegFormer) surpass previous methods by large margin on results of “Car” category.

As shown in Fig.6, we provide the visualization results on LoveDA dataset. Since images in testing dataset do not have annotations, we display the results of images in validation dataset. It can be seen that ST-DASegNet can produce reasonable predictions. Especially on some hard categories like “Barren” and “Forest”, ST-DASegNet can also predict well. The visualization results also coincide with the results in Tab.V and Tab.VI.

2) *Visual ablation study:* To separately show the effectiveness of key components of ST-DASegNet in an intuitive manner, we provide ablation visualization on “Potsdam IR-R-G to Vaihingen IR-R-G” and “Potsdam R-G-B to Vaihingen IR-R-G” tasks shown in Fig.7. When adding DDM, many large-region mistakes are avoided. In baseline result of case (b), large regions of “Low vegetation” are classified into “Tree”. In baseline result of case (c), large regions of “Clutter” are classified into “Building”. After adding DDM, these large-region mistakes are correctly classified. When adding adversarial learning, the edge of each category is clearer and the whole region of each category becomes smoothly. In all 6 cases, we find that many small regions will be incorrectly classified into “Clutter”. After adding adversarial learning, this problem is almost completely solved. When further applying EMA based cross-domain separated self-training mechanism, many detailed mistakes for almost every categories are corrected, which makes the results seem much better. As shown in case (a), (b) and (f), some little rectifications on “Building” make predictions seem closer to ground truth. Similarly in case (b) and (e), detailed corrections on “Impervious surfaces” really help improve the quality predictions.

Theoretically, with DDM, source and target student backbones can respectively represent the target images into source-style and target-style with only source annotations. In other words, besides domain universal features, some target-specific features can be extracted. However, feature inconsistency caused from domain shift will harm the effectiveness of DDM. When further adding feature-level adversarial learning, domain shift problem is eased and cross-domain single-style features is aligned to become more consist. Therefore, feature representation capability of backbones and DDM are both improved. When integrating our proposed self-training mechanism, it can fundamentally improve this task by providing high-quality target annotations. In summary, besides ablation comparison experiments (Tab.VII and Tab.VIII), ablation visualization further prove the effectiveness and great compatibility of the three key components of ST-DASegNet.

3) *Visualization and analysis on feature maps:* To intuitively show the interpretability of ST-DASegNet, we visualize

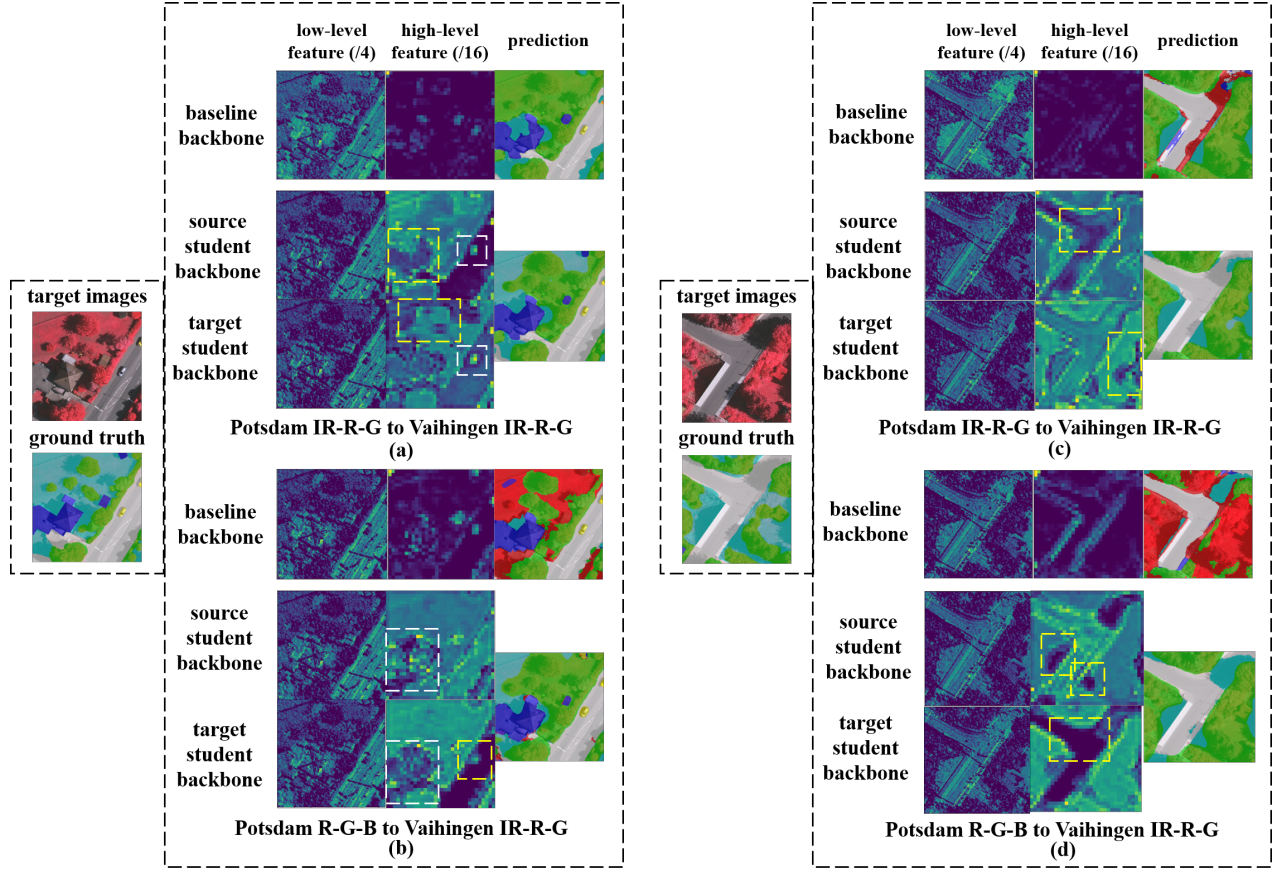


Fig. 8. Feature map visualization comparison between baseline model and ST-DASegNet. We select the feature maps extracted from backbones for visualization. Feature maps listed here are channel-wise average feature maps. “/4” and “/16” respectively indicates the downsampling rate compared to original image. “Prediction” indicates final segmentation results of baseline model and ST-DASegNet.

the multi-level feature maps extracted from backbones and make analysis. We select “Potsdam IR-R-G to Vaihingen IR-R-G” and “Postdam R-G-B to Vaihingen IR-R-G” tasks to conduct experiments. We select SegFormer as baseline model.

Feature map visualization comparison between baseline model and ST-DASegNet. As shown in Fig.8, we will analyze the visualization results with 2 cases from the following 2 points. (1) Baseline model and ST-DASegNet both have well-represented low-level feature maps, which have abundant detailed information and clear edges among regions of each category. (2) On high-level feature maps, it is obvious that two backbones of ST-DASegNet has better representation capability than baseline backbones. As shown in the “yellow box” region of case (a), ST-DASegNet’s high-level feature maps have clearer boundaries between regions of “Tree” and “Low vegetation”. As shown in case (a) and case (b), we find that the edge of “Building” on ST-DASegNet’s high-level feature maps is also in better shape. Case (c) and case (d) reveal that ST-DASegNet has better performance on localizing “Low vegetation”. From 4 cases in Fig.8, we find that the high-level feature maps of baseline backbone will miss some important information. Even though baseline backbone can represent well on some categories (e.g. Impervious surfaces in case (d)), the generalized representation ability is far behind ST-DASegNet.

Feature map visualization comparison between source and target student backbones of ST-DASegNet. Cases in Fig.8 intuitively prove the effectiveness of our dual backbones structure. First, the two backbones of ST-DASegNet are complementary in representing target images. As shown in the “yellow box” region of case (a), source student backbone can better find the “Building” edges while target student backbone can better distinguish the boundaries between regions of “Tree” and “Low vegetation”. In case (b), when source student backbone fails to localize “Car”, target student backbone successfully find it. In case (c) and (d), one backbone has advantages on dividing the edge of “Impervious surfaces” and the other has better performance on recognizing “Low vegetation”. Second, two backbones can extract universal features. As shown in the “white box” regions of case (a) and (b), two backbones respectively have strong perception on “Car” and “Building”. Third, source and target student backbones in ST-DASegNet can respectively represent target images in source-style and target-style. In case (a), we find that source student backbone tends to focus on “Building” and “Impervious surfaces”, which is similar to source-only trained baseline model. Target student backbone tends to have better focus on “Low vegetation”, because intuitive distinguishing “Low vegetation” and “Tree” in target images (Vaihingen IR-R-G) is easier than source images (Potsdam IR-R-G). From

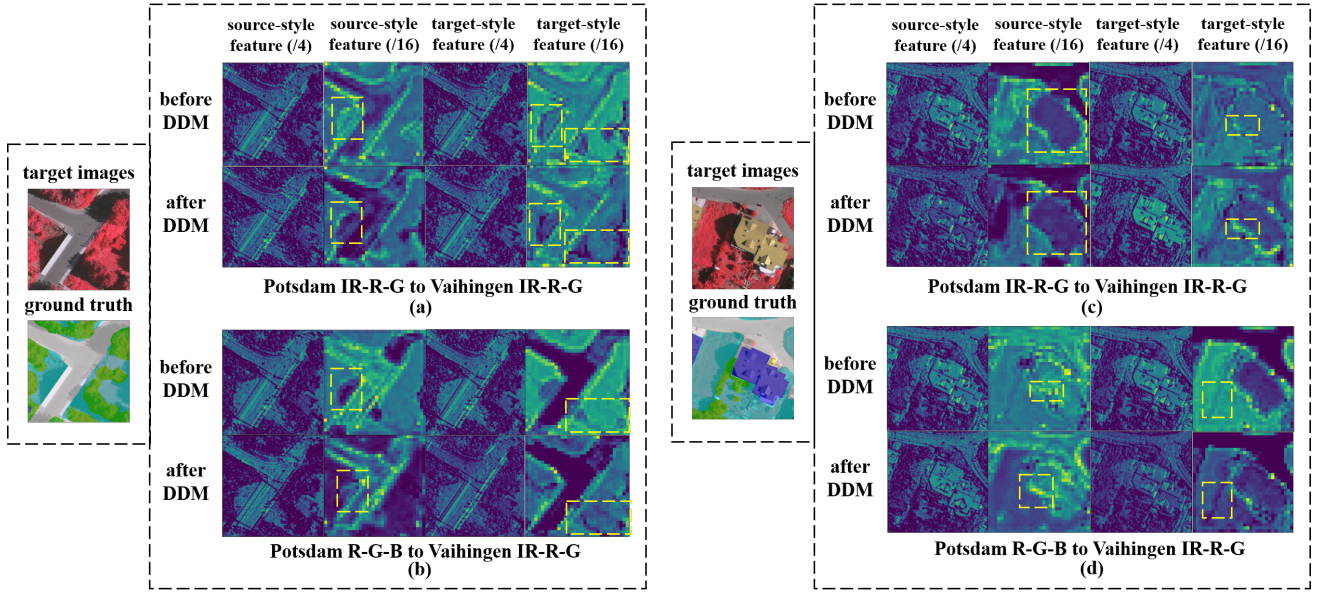


Fig. 9. Visualization on domain disentangling. We select the feature maps extracted from backbones for visualization. Feature maps listed here are channel-wise average feature maps. “/4” and “/16” respectively indicates the downsampling rate compared to original image.

another perspective, if comparing case (c) with case (d), we find the representation style (preference) of source style backbone completely changes, because source-domain images change from Potsdam IR-R-G from Potsdam R-G-B.

Visualization on domain disentangling. Achieving high-quality domain disentangling with DDM is important for ST-DASegNet. With DDM, we expect to extract the universal feature and purify the distinct feature of source-style and target-style features. If DDM works well, more distinct target-style feature extraction can make effect on better representing target images and more difference between source-style and target-style feature extraction can improve the representation diversity. In Fig.9, we adopt feature map visualization comparison to intuitively analyze domain disentangling. First, Low-level features have minor changes because low-level features are always invariant, similar and “no-style”. Second, after DDM, high-level source-style and target-style features both become more distinct. In case (a) and (c), we observe that high-level source-style feature tends to focus on “Impervious surfaces” and “Building”, which is also proved in Fig.8. After DDM, the boundary of “Impervious surfaces” becomes clearer and expanded (case (a)). The expanded part is shadow and source student backbone tends to recognize it as “Impervious surfaces”. Moreover, after DDM, the boundary of “Building” is in better shape (case (c)). As a complementary, target-style feature tends to focus on “Low vegetation” and “Tree”. The features after DDM obviously have more tendency on these two categories (case (a) and (c)). Particularly on the shadow area in case (a), target student backbone tends to recognize it as “Low vegetation”. Case (b) and case (d) also show that high-level source-style and target-style features become more distinct and different from each other, which proves the effectiveness of our proposed domain disentangling mechanism.

V. CONCLUSION

In this paper, we propose a self-training guided disentangled adaptation method (ST-DASegNet) to tackle cross-domain remote sensing image semantic segmentation. In ST-DASegNet, we propose a dual path structure with two student backbones and two student decoders, which aims to represent source and target images into source-style and target-style with only source annotations. Based on this structure, we propose feature-level adversarial learning on cross-domain single-style features to enhance the representation consistency by feature alignment mechanism. Furthermore, we propose domain disentangled module (DDM) on single-domain cross-style features to make source-style and target-style features more distinct and diverse. Besides adversarial learning and DDM, we propose and integrate EMA based cross-domain separated self-training paradigm (“Decoder-only” and “Single-target”). Our proposed self-training mechanism can balance the representation tendency between source and target domains by generating pseudo-labels of target images. The three key components show great compatibility, which can improve the performance of ST-DASegNet in three different perspectives. Extensive experiments on different benchmark datasets show that ST-DASegNet outperforms the previous SOTA methods on cross-domain RS image semantic segmentation task. Abundant visualization analysis intuitively prove that our proposed ST-DASegNet are reasonable and interpretable.

ACKNOWLEDGMENT

This work was supported by the National Natural Science Foundation of China (grant number 62072021 and 61901015).

REFERENCES

- [1] G. Xia, J. Hu, F. Hu *et al.*, “Aid: A benchmark data set for performance evaluation of aerial scene classification,” *IEEE Transactions on Geoscience and Remote Sensing*, vol. 55, no. 7, pp. 3965–3981, 2017.

- [2] Y. Yang and S. D. Newsam, "Bag-of-visual-words and spatial extensions for land-use classification," in *Sigspatial International Symposium on Advances in Geographic Information Systems*, 2010, pp. 270–279.
- [3] G. Cheng, J. Han, and X. Lu, "Remote sensing image scene classification: Benchmark and state of the art," *Proceedings of the IEEE*, vol. 105, no. 10, pp. 1865–1883, 2017.
- [4] Q. Zhao, S. Lyu, Y. Li *et al.*, "Mgm1: Multigranularity multilevel feature ensemble network for remote sensing scene classification," *IEEE Transactions on Neural Networks and Learning Systems*, 2021. [Online]. Available: 10.1109/TNNLS.2021.3106391
- [5] Q. Wang, W. Huang, Z. Xiong *et al.*, "Looking closer at the scene: Multiscale representation learning for remote sensing image scene classification," *IEEE Transactions on Neural Networks and Learning Systems*, vol. 33, no. 4, pp. 1414–1428, 2022.
- [6] G. Xia, X. Bai, J. Ding *et al.*, "DOTA: A large-scale dataset for object detection in aerial images," in *IEEE Conference on Computer Vision and Pattern Recognition*, 2018, pp. 3974–3983.
- [7] J. Ding, N. Xue, Y. Long *et al.*, "Learning roi transformer for detecting oriented objects in aerial images," in *IEEE Conference on Computer Vision and Pattern Recognition*, 2019, pp. 2844–2853.
- [8] Q. Lin, J. Zhao, G. Fu *et al.*, "Crpn-sfnet: A high-performance object detector on large-scale remote sensing images," *IEEE Transactions on Neural Networks and Learning Systems*, vol. 33, no. 1, pp. 416–429, 2022.
- [9] Y. Lyu, G. Vosselman, G.-S. Xia *et al.*, "Uavid: A semantic segmentation dataset for uav imagery," *ISPRS Journal of Photogrammetry and Remote Sensing*, vol. 165, pp. 108–119, 2020.
- [10] J. Hou, Z. Guo, Y. Wu *et al.*, "Bsnet: Dynamic hybrid gradient convolution based boundary-sensitive network for remote sensing image segmentation," *IEEE Transactions on Geoscience and Remote Sensing*, vol. 60, pp. 1–22, 2022.
- [11] Q. Zhao, J. Liu, Y. Li *et al.*, "Semantic segmentation with attention mechanism for remote sensing images," *IEEE Transactions on Geoscience and Remote Sensing*, vol. 60, pp. 1–13, 2022.
- [12] E. Shelhamer, J. Long, and T. Darrell, "Fully convolutional networks for semantic segmentation," *IEEE Transactions on Pattern Analysis and Machine Intelligence*, vol. 39, no. 4, pp. 640–651, 2017.
- [13] H. Zhao, J. Shi, X. Qi *et al.*, "Pyramid scene parsing network," in *IEEE Conference on Computer Vision and Pattern Recognition*, 2017, pp. 6230–6239.
- [14] L. Chen, Y. Zhu, G. Papandreou *et al.*, "Encoder-decoder with atrous separable convolution for semantic image segmentation," in *European Conference on Computer Vision*, vol. 11211, 2018, pp. 833–851.
- [15] E. Xie, W. Wang, Z. Yu *et al.*, "Segformer: Simple and efficient design for semantic segmentation with transformers," in *Advances in Neural Information Processing Systems*, vol. 34, 2021, pp. 12 077–12 090.
- [16] Y. Cai, L. Dai, H. Wang *et al.*, "Dlnet with training task conversion stream for precise semantic segmentation in actual traffic scene," *IEEE Transactions on Neural Networks and Learning Systems*, vol. 33, no. 11, pp. 6443–6457, 2022.
- [17] Y. Tsai, W. Hung, S. Schuster *et al.*, "Learning to adapt structured output space for semantic segmentation," in *IEEE Conference on Computer Vision and Pattern Recognition*, 2018, pp. 7472–7481.
- [18] J. Hoffman, E. Tzeng, T. Park *et al.*, "Cycada: Cycle-consistent adversarial domain adaptation," in *International Conference on Machine Learning*, vol. 80, 2018, pp. 1994–2003.
- [19] J. Zhu, T. Park, P. Isola *et al.*, "Unpaired image-to-image translation using cycle-consistent adversarial networks," in *IEEE International Conference on Computer Vision*, 2017, pp. 2242–2251.
- [20] Q. Zhou, Z. Feng, Q. Gu *et al.*, "Uncertainty-aware consistency regularization for cross-domain semantic segmentation," *Computer Vision and Image Understanding*, vol. 221, p. 103448, 2022.
- [21] L. Hoyer, D. Dai, and L. V. Gool, "Daformer: Improving network architectures and training strategies for domain-adaptive semantic segmentation," in *IEEE Conference on Computer Vision and Pattern Recognition*. IEEE, 2022, pp. 9914–9925.
- [22] M. Gerke, "Use of the stair vision library within the isprs 2d semantic labeling benchmark (vaihingen)," ITC, Univ. Twente, Enschede, The Netherlands, Tech. Rep., 2014, doi: 10.13140/2.1.5015.9683.
- [23] J. Wang, Z. Zheng, A. Ma *et al.*, "Loveda: A remote sensing land-cover dataset for domain adaptive semantic segmentation," in *Neural Information Processing Systems*, 2021.
- [24] V. Badrinarayanan, A. Kendall, and R. Cipolla, "Segnet: A deep convolutional encoder-decoder architecture for image segmentation," *IEEE Transactions on Pattern Analysis and Machine Intelligence*, vol. 39, no. 12, pp. 2481–2495, 2017.
- [25] J. Fu, J. Liu, H. Tian *et al.*, "Dual attention network for scene segmentation," in *IEEE Conference on Computer Vision and Pattern Recognition*, 2019, pp. 3146–3154.
- [26] Z. Huang, X. Wang, L. Huang *et al.*, "Ccnet: Criss-cross attention for semantic segmentation," in *IEEE International Conference on Computer Vision*. IEEE, 2019, pp. 603–612.
- [27] T. Wu, S. Tang, R. Zhang *et al.*, "Cgnet: A light-weight context guided network for semantic segmentation," *IEEE Transactions on Image Processing*, vol. 30, pp. 1169–1179, 2021.
- [28] C. Yu, C. Gao, J. Wang *et al.*, "Bisenet V2: bilateral network with guided aggregation for real-time semantic segmentation," *International Journal of Computer Vision*, vol. 129, no. 11, pp. 3051–3068, 2021.
- [29] G. Li, L. Li, H. Zhu, X. Liu *et al.*, "Adaptive multiscale deep fusion residual network for remote sensing image classification," *IEEE Transactions on Geoscience and Remote Sensing*, vol. 57, no. 11, pp. 8506–8521, 2019.
- [30] K. Nogueira, M. D. Mura, J. Chanussot *et al.*, "Dynamic multicontext segmentation of remote sensing images based on convolutional networks," *IEEE Transactions on Geoscience and Remote Sensing*, vol. 57, no. 10, pp. 7503–7520, 2019.
- [31] L. Mou, Y. Hua, and X. Zhu, "Relation matters: Relational context-aware fully convolutional network for semantic segmentation of high-resolution aerial images," *IEEE Transactions on Geoscience and Remote Sensing*, vol. 58, pp. 7557–7569, 2020.
- [32] H. Li, K. Qiu, L. Chen, X. Mei, L. Hong, and C. Tao, "Scattnet: Semantic segmentation network with spatial and channel attention mechanism for high-resolution remote sensing images," *IEEE Geoscience and Remote Sensing Letters*, vol. 18, pp. 905–909, 2021.
- [33] Q. Zhao, J. Liu, Y. Li *et al.*, "Semantic segmentation with attention mechanism for remote sensing images," *IEEE Transactions on Geoscience and Remote Sensing*, vol. 60, pp. 1–13, 2022.
- [34] S. Liu, W. Ding, C. Liu *et al.*, "Ern: Edge loss reinforced semantic segmentation network for remote sensing images," *Remote Sensing*, vol. 10, p. 1339, 2018.
- [35] G. Yang, Q. Zhang, and G. Zhang, "Eanet: Edge-aware network for the extraction of buildings from aerial images," *Remote Sensing*, vol. 12, no. 13, p. 2161, 2020.
- [36] A. Li, L. Jiao, H. Zhu, L. Li, and F. Liu, "Multitask semantic boundary awareness network for remote sensing image segmentation," *IEEE Transactions on Geoscience and Remote Sensing*, vol. 60, pp. 1–14, 2022.
- [37] J. Hou, Z. Guo, Y. Wu, W. Diao, and T. Xu, "Bsnet: Dynamic hybrid gradient convolution based boundary-sensitive network for remote sensing image segmentation," *IEEE Transactions on Geoscience and Remote Sensing*, vol. 60, pp. 1–22, 2022.
- [38] P. Isola, J. Zhu, T. Zhou *et al.*, "Image-to-image translation with conditional adversarial networks," in *IEEE Conference on Computer Vision and Pattern Recognition*, 2017, pp. 5967–5976.
- [39] Y. Chen, W. Li, X. Chen *et al.*, "Learning semantic segmentation from synthetic data: A geometrically guided input-output adaptation approach," in *IEEE Conference on Computer Vision and Pattern Recognition*, 2019, pp. 1841–1850.
- [40] Y. Yang and S. Soatto, "FDA: fourier domain adaptation for semantic segmentation," in *IEEE Conference on Computer Vision and Pattern Recognition*, 2020, pp. 4084–4094.
- [41] S. Guo, Q. Zhou *et al.*, "Label-free regional consistency for image-to-image translation," in *IEEE International Conference on Multimedia and Expo*, 2021, pp. 1–6.
- [42] C. Chen, Q. Dou, H. Chen *et al.*, "Unsupervised bidirectional cross-modality adaptation via deeply synergistic image and feature alignment for medical image segmentation," *IEEE Transactions Medical Imaging*, vol. 39, no. 7, pp. 2494–2505, 2020.
- [43] D. Zou, Q. Zhu, and P. Yan, "Unsupervised domain adaptation with dual-scheme fusion network for medical image segmentation," in *International Joint Conference on Artificial Intelligence*, 2020, pp. 3291–3298.
- [44] Y. Tsai, W. Hung, S. Schuster *et al.*, "Learning to adapt structured output space for semantic segmentation," in *IEEE Conference on Computer Vision and Pattern Recognition*, 2018, pp. 7472–7481.
- [45] L. Du, J. Tan, H. Yang *et al.*, "SSF-DAN: separated semantic feature based domain adaptation network for semantic segmentation," in *IEEE International Conference on Computer Vision*, 2019, pp. 982–991.
- [46] H. Wang, T. Shen, W. Zhang, L.-Y. Duan, and T. Mei, "Classes matter: A fine-grained adversarial approach to cross-domain semantic segmentation," in *European Conference on Computer Vision*, 2020.
- [47] G. Zeng, F. Schmaranzer, T. D. Lerch *et al.*, "Entropy guided unsupervised domain adaptation for cross-center hip cartilage segmentation

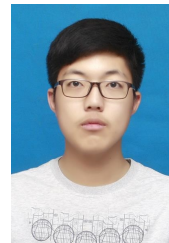
- from MRI,” in *Medical Image Computing and Computer Assisted Intervention*, vol. 12261, 2020, pp. 447–456.
- [48] Y. Zou, Z. Yu, X. Liu *et al.*, “Confidence regularized self-training,” *IEEE International Conference on Computer Vision*, pp. 5981–5990, 2019.
- [49] Q. Zhou, C. Zhuang, X. Lu *et al.*, “Domain adaptive semantic segmentation via regional contrastive consistency regularization,” *IEEE International Conference on Multimedia and Expo*, pp. 01–06, 2022.
- [50] B. Benjdira, Y. Bazi, A. Koubâa *et al.*, “Unsupervised domain adaptation using generative adversarial networks for semantic segmentation of aerial images,” *Remote Sensing*, vol. 11, p. 1369, 2019.
- [51] Y. Li, T. Shi, Y. Zhang *et al.*, “Learning deep semantic segmentation network under multiple weakly-supervised constraints for cross-domain remote sensing image semantic segmentation,” *Isprs Journal of Photogrammetry and Remote Sensing*, vol. 175, pp. 20–33, 2021.
- [52] Z. Yi, H. Zhang, P. Tan *et al.*, “Dualgan: Unsupervised dual learning for image-to-image translation,” *IEEE International Conference on Computer Vision*, pp. 2868–2876, 2017.
- [53] X. Chen, S. Pan, and Y. Chong, “Unsupervised domain adaptation for remote sensing image semantic segmentation using region and category adaptive domain discriminator,” *IEEE Transactions on Geoscience and Remote Sensing*, vol. 60, pp. 1–13, 2022.
- [54] J. Chen, J. Zhu, Y. Guo *et al.*, “Unsupervised domain adaptation for semantic segmentation of high-resolution remote sensing imagery driven by category-certainty attention,” *IEEE Transactions on Geoscience and Remote Sensing*, vol. 60, pp. 1–15, 2022.
- [55] Y. Zhao, H. Gao, P. Guo *et al.*, “Residualgan: Resize-residual dualgan for cross-domain remote sensing images semantic segmentation,” *ArXiv*, vol. abs/2201.11523, 2022.
- [56] L. Bai, S. Du, X. Zhang *et al.*, “Domain adaptation for remote sensing image semantic segmentation: An integrated approach of contrastive learning and adversarial learning,” *IEEE Transactions on Geoscience and Remote Sensing*, vol. 60, pp. 1–13, 2022.
- [57] L. Wu, M. Lu, and L. Fang, “Deep covariance alignment for domain adaptive remote sensing image segmentation,” *IEEE Transactions on Geoscience and Remote Sensing*, vol. 60, pp. 1–11, 2022.
- [58] J. Li, S. Zi, R. Song *et al.*, “A stepwise domain adaptive segmentation network with covariate shift alleviation for remote sensing imagery,” *IEEE Transactions on Geoscience and Remote Sensing*, vol. 60, pp. 1–15, 2022.
- [59] B. Zhang, T. Chen, and B. Wang, “Curriculum-style local-to-global adaptation for cross-domain remote sensing image segmentation,” *IEEE Transactions on Geoscience and Remote Sensing*, vol. 60, pp. 1–12, 2022.
- [60] S. Ji, D. Wang, and M. Luo, “Generative adversarial network-based full-space domain adaptation for land cover classification from multiple-source remote sensing images,” *IEEE Transactions on Geoscience and Remote Sensing*, vol. 59, no. 5, pp. 3816–3828, 2021.
- [61] P. Zhang, B. Zhang, T. Zhang *et al.*, “Prototypical pseudo label denoising and target structure learning for domain adaptive semantic segmentation,” in *IEEE Conference on Computer Vision and Pattern Recognition*, 2021, pp. 12414–12424.
- [62] K. He, X. Zhang, S. Ren, and J. Sun, “Deep residual learning for image recognition,” in *IEEE Conference on Computer Vision and Pattern Recognition*, 2016, pp. 770–778.
- [63] P. Isola, J. Zhu, T. Zhou *et al.*, “Image-to-image translation with conditional adversarial networks,” in *IEEE Conference on Computer Vision and Pattern Recognition*, 2017, pp. 5967–5976.
- [64] E. Tzeng, J. Hoffman, N. Zhang *et al.*, “Deep domain confusion: Maximizing for domain invariance,” *CoRR*, vol. abs/1412.3474, 2014.
- [65] H. Wang, T. Shen, W. Zhang *et al.*, “Classes matter: A fine-grained adversarial approach to cross-domain semantic segmentation,” in *European Conference on Computer Vision*, vol. 12359, 2020, pp. 642–659.
- [66] Y. Luo, L. Zheng, T. Guan *et al.*, “Taking a closer look at domain shift: Category-level adversaries for semantics consistent domain adaptation,” in *IEEE Conference on Computer Vision and Pattern Recognition*, 2019, pp. 2507–2516.
- [67] J. Wang, Y. Zhong, Z. Zheng *et al.*, “Rsnets: The search for remote sensing deep neural networks in recognition tasks,” *IEEE Transactions on Geoscience and Remote Sensing*, vol. 59, no. 3, pp. 2520–2534, 2021.
- [68] Q. Lian, L. Duan, F. Lv *et al.*, “Constructing self-motivated pyramid curriculums for cross-domain semantic segmentation: A non-adversarial approach,” in *IEEE International Conference on Computer Vision*, 2019, pp. 6757–6766.
- [69] Y. Zou, Z. Yu, B. V. K. V. Kumar *et al.*, “Unsupervised domain adaptation for semantic segmentation via class-balanced self-training,” in *European Conference on Computer Vision*, vol. 11207, 2018, pp. 297–313.
- [70] K. Mei, C. Zhu, J. Zou *et al.*, “Instance adaptive self-training for unsupervised domain adaptation,” in *European Conference on Computer Vision*, vol. 12371, 2020, pp. 415–430.



Qi Zhao received Ph.D in communication and information system from Beihang University, Beijing, China. She is a professor and works in Beihang University. She was in the Department of Electrical and Computer Engineering at the University of Pittsburgh as a visiting scholar from 2014 to 2015. Since 2016, she has been working on wearable device based first-view image processing and deep learning based image recognition. Her current research interests include RS image semantic segmentation, signal processing and target tracking.



Shuchang Lyu received the B.S. degree in Department of Communication and Information from Shanghai University, Shanghai, China, in 2016, and the M.E. from Department of Electronic and Information Engineering, Beihang University, Beijing, China, in 2019. Currently, he is pursuing the Ph.D. degree in Department of Electronic and Information Engineering, Beihang University, Beijing. His current research interests include domain adaptation semantic segmentation, RS image understanding, high-efficiency network design.



Binghao Liu received B.E. degree in electronics and information engineering from Beihang University, Beijing, China, in 2019. He is currently pursuing the Ph.D. degree with the School of Electronic and Information Engineering, Beihang University, Beijing. His research interests include weakly supervised learning, semantic segmentation and few-shot semantic segmentation.



Lijiang Chen respectively received B.S. and Ph.D. degrees in Department of Electronic and Information Engineering from Beihang University in 2007 and 2012. Currently, he is an assistant professor with Department of Electronic and Information Engineering, Beihang University. His current research interests include natural language processing, medical image understanding and human-computer interaction.



Hongbo Zhao received a B.S. degree and a Ph.D. degree in electronic engineering from Beihang University in 2006 and 2012, respectively. He is now a professor with Beihang University. His research focuses on integrated remote sensing and communication.